

AGH

AKADEMIA GÓRNICZO-HUTNICZA IM. STANISŁAWA STASZICA W KRAKOWIE

**WYDZIAŁ INFORMATYKI, ELEKTRONIKI I TELEKOMUNIKACJI
KATEDRA ELEKTRONIKI**

PRACA DYPLOMOWA INŻYNIERSKA

**TOTAL IONIZING DOSE (TID) SENSOR FOR
CUBESENT NANO-SATELLITES**

**BUDOWA SENSORA POCHŁONIĘTEJ DAWKI PROMIENIOWANIA
JONIZUJĄCEGO (TID) DLA NANO-SATELITÓW TYPU CUBESENT**

AUTOR: Grzegorz Gajoch

KIERUNEK STUDIÓW: Elektronika i Telekomunikacja

PIEKUN PRACY: dr inż. Cezary Worek

Kraków 2016

OŚWIADCZENIE AUTORA PRACY

UPRZEDZONY O ODPOWIEDZIALNOŚCI KARNEJ NA PODSTAWIE ART. 115 UST. 1 I 2 USTAWY Z DNIA 4 LUTEGO 1994 R. O PRAWIE AUTORSKIM I PRAWACH POKREWNYCH (T.J. Dz.U. z 2006 r. Nr 90, poz. 631 z późn. zm.): „KTO PRZYWŁASZCZA SOBIE AUTORSTWO ALBO WPROWADZA W BŁĄD CO DO AUTORSTWA CAŁOŚCI LUB CZĘŚCI CUDZEGO UTWORU ALBO ARTYSTYCZNEGO WYKONANIA, PODLEGA GRZYWNIE, KARZE OGRANICZENIA WOLNOŚCI ALBO POZBAWIENIA WOLNOŚCI DO LAT 3. TEJ SAMEJ KARZE PODLEGA, KTO ROZPOWSZECHNIA BEZ PODANIA NAZWISKA LUB PSEUDONIMU TWÓRCY CUDZY UTWÓR W WERSJI ORYGINALNEJ ALBO W POSTACI OPRACOWANIA, ARTYSTYCZNE WYKONANIE ALBO PUBLICZNIE ZNIEKSZTAŁCA TAKI UTWÓR, ARTYSTYCZNE WYKONANIE, FONOGRAM, VIDEOGRAM LUB NADANIE.”, A TAKŻE UPRZEDZONY O ODPOWIEDZIALNOŚCI DYSCYPLINARNEJ NA PODSTAWIE ART. 211 UST. 1 USTAWY Z DNIA 27 LIPCA 2005 R. PRAWO O SZKOLNICTWIE WYŻSZYM (T.J. Dz. U. z 2012 r. poz. 572, z późn. zm.) „ZA NARUSZENIE PRZEPISÓW OBOWIĄZUJĄCYCH W UCZELNI ORAZ ZA CZYNY UCHYBIAJĄCE GODNOŚCI STUDENTA STUDENT PONOSI ODPOWIEDZIALNOŚĆ DYSCYPLINARNĄ PRZED KOMISJĄ DYSCYPLINARNĄ ALBO PRZED SĄDEM KOLEŻEŃSKIM SAMORZĄDU STUDENCKIEGO, ZWANYM DALEJ „SĄDEM KOLEŻEŃSKIM”, OŚWIADCZAM, ŻE NINIEJSZĄ PRACĘ DYPLOMOWĄ WYKONAŁEM(-AM) OSOBIŚCIE, SAMODZIELNIE I ŻE NIE KORZYSTAŁEM(-AM) ZE ŹRÓDEŁ INNYCH NIŻ WYMIESZCZONE W PRACY.

.....
PODPIS

Contents

1. Definitions and abbreviated terms.....	7
1.1. Definitions	7
1.2. Abbreviations.....	8
2. Introduction.....	10
3. Principles	12
3.1. Radiation on Low Earth Orbit	12
3.2. Radiation effects on electronic devices	13
3.2.1. Single Event Effects.....	13
3.2.2. Total Ionizing Dose	15
3.3. Need for TID radiation dosimetry	15
3.4. On-line TID radiation dosimetry	15
3.5. RadFET Theory	16
3.5.1. Radiation effects on MOS transistors	16
3.5.2. Threshold voltage measurement	17
3.5.3. Temperature dependencies	18
4. Design requirements	19
4.1. PW-Sat2	19
4.1.1. Primary mission	20
4.1.2. Lifetime.....	21
4.1.3. Orbit	21
4.1.4. Radiation analysis	21
4.2. Sensor requirements	22
4.3. Applicable standards	22
4.4. Electrical requirements	23

4.4.1. Electronics stack	23
4.4.2. PC-104 connector.....	24
4.4.3. Power rail.....	24
4.4.4. Power consumption.....	24
4.4.5. Data interface	24
4.4.6. Radiation immunity.....	24
4.4.7. Electromagnetic compatibility	25
4.4.8. Inrush current	26
4.4.9. Reliability of components	26
4.5. Mechanical requirements.....	26
4.5.1. PCB	26
4.5.2. Outgassing.....	27
4.5.3. Vibration.....	27
4.5.4. Operation temperature.....	28
4.5.5. Thermal cycles	28
5. Sensor design	29
5.1. Review of commercially available RadFETs	29
5.2. COTS MOSFET as RadFET	30
5.3. Selected MOSFET - CD4007	31
5.4. Threshold voltage measurement.....	32
5.5. Temperature measurement.....	32
5.6. Characteristic curves.....	34
5.7. Operating point selection.....	35
6. Engineering model	36
6.1. Background - calibration stand.....	36
6.2. Block diagram	36
6.3. Low-level requirements	37
6.4. Analog front-end	38
6.4.1. SPICE models	38
6.4.2. Linear regulator	38
6.4.3. RadFET power switch.....	39

6.4.4. Current source	39
6.4.5. Analog to digital converter.....	42
6.4.6. Multiplexer.....	44
6.4.7. Differential & common mode filter.....	45
6.4.8. Shielding	46
6.5. Digital	46
6.5.1. Microcontroller	46
6.5.2. On-Board Computer interface.....	47
6.5.3. Watchdog.....	48
6.6. Final schematic	49
6.7. PCB.....	49
6.7.1. PCB materials	49
6.7.2. PCB stack.....	50
6.7.3. PCB layout	50
6.7.4. 3D model.....	52
6.8. Software design	52
6.8.1. AVR-HAL	53
6.8.2. I^2C -slave interface	54
6.8.3. Measurement algorithm	54
6.9. Assembly	55
6.10. Finished sensor	56
7. Sensor tests	57
7.1. Power.....	57
7.1.1. LDO stabilisation	57
7.1.2. Power consumption.....	57
7.2. Current source	58
7.2.1. Noise	58
7.2.2. Load range.....	59
7.2.3. Temperature stability.....	59
7.3. MOS settling.....	60
7.4. Measurement noise.....	60

7.4.1. Diode	61
7.4.2. Threshold voltage.....	62
7.4.3. Interpretation.....	63
7.5. Temperature characteristics	63
7.5.1. Diode channel	63
7.5.2. Threshold voltage channels.....	64
7.6. Temperature compensation stability.....	65
8. Future work.....	66
8.1. Qualification model	66
8.2. Flight model.....	67
9. Summary.....	68

1. Definitions and abbreviated terms

1.1. Definitions

- **Total ionizing dose** – the portion of the energy absorbed by a matter during the whole time of exposure on ionizing radiation. [27] Expressed in grays (Gy) or rads (Rad). 1 Gy = 100 rad.
- **CubeSat** – a nano-satellite, composed of multiples 10 x 10 x 11.35 cm cubic units, each of a 1.33 kg mass. Frequently build by university students, for educational and research purposes. [8]
- **RadFET** – common name for specialized, radiation sensitive P-MOSFET transistors used in TID measurements.
- **Low Earth orbit** – an orbit with an altitude between 180 km and 2000 km. Most scientific and observatory satellites are located at the Low Earth Orbit. [35]
- **Dosimeter** – a sensor that measures exposure to ionising radiation.
- **PW-Sat2** – second CubeSat, undergoing building on Warsaw University of Technology, scheduled to be launched on Q4 2017.
- **Engineering model** – This model is form, fit, and functionally the same as the final flight model; however, it will use a mixture of flight-grade components (usually spare or out-of-life in stores) and commercial components. [39]
- **Qualification model** – This is the model that is subjected to the qualification campaign. This usually includes design updates from the EM and uses identical components to flight; however, these components do not need to be screened to the flight standard. [39]
- **Flight model** – The models actually flying; these are tested to acceptance-level testing. [39]
- **COTS** – Components which are adapted to satisfy the needs of the purchasing organization, rather than the commissioning of custom made solutions, especially in high-reliability designs.

1.2. Abbreviations

- **ADC** – Analog to Digital Converter
- **API** – Application Programming Interface
- **ASIC** – Application Specific Integrated Circuit
- **COTS** – Commercial Off-The-Shelf
- **DC** – Direct Current
- **DUT** – Device Under Test
- **ECSS** – European Cooperation for Space Standardization
- **EMC** – Electromagnetic Compatibility
- **EMI** – Electromagnetic Interference
- **EPS** – Electrical Power Supply
- **ESCIES** – European Space Components Information Exchange System
- **ESD** – Electrostatic Discharge
- **FDIR** – Fault Detection, Isolation and Recovery
- **GPIO** – General Purpose Input Output
- **HAL** – Hardware Abstraction Layer
- **I²C** – Inter-Integrated Circuit
- **I/O** – Input/Output
- **LCL** – Latch-up Current Limiter
- **LDO** – Low-Dropout linear regulator
- **LEO** – Low Earth Orbit
- **LET** – Linear Energy Transfer
- **LSB** – Least Significant Bit
- **LTAN** – Local Time Ascending Node

- **MCU** – Micro-Controller Unit
- **MOSFET** – Metal–Oxide–Semiconductor Field-Effect Transistor
- **MUX** – Multiplexer
- **OBC** – On-Board Computer
- **PCB** – Printed Circuit Board
- **PLD** – Payload
- **PSRR** – Power supply rejection ratio
- **RF** – Radio Frequencies
- **RMS** – Root-Mean Squared
- **RadFET** – Radiation Sensitive Field Effect Transistor
- **SAA** – South Atlantic Anomaly
- **SEE** – Single Event Effect
- **SEL** – Single Event Latch-up
- **SEU** – Single Event Upset
- **SMD** – Surface Mounted Device
- **TID** – Total Ionizing Dose
- **ZTC** – Zero Temperature Coefficient

2. Introduction

Ionizing radiation is one of the major concerns during space mission development, both manned and unmanned. Just as the human body is affected by radiation, so are electronic components, which will fail under certain conditions.

A special design methodology, radiation hardening, must be implemented for all satellite components, which dramatically increases mission costs. Some assumptions are made during satellite planning, such as radiation tolerance, above which the mission can fail. Absorbed dose can be predicted by simulations, but unusual events like solar flares can alter predictions to unacceptable levels. For monitoring the absorbed dose, most satellites have on-board Total Ionizing Dose (TID) sensors, allowing to deorbit or move satellite to graveyard orbit before it fails.

Usually, these sensors are very expensive and it is hard to cut the cost due to custom ASIC design. They are also large and require a lot of power to operate. However, recent publications suggest that Commercial Off-The-Shelf (COTS) transistors can be used to assemble an absorbed dose sensor.

To date, very few small student-satellites (e.g. CubeSats) have TID sensors on-board. This is mainly due to their cost, but also to limited time, space and power resources. At present, this sensor is not critical in Low Earth Orbit (LEO), when, following failure, a satellite will deorbit by means of atmospheric drag. In the near future, as a consequence of expanding CubeSat market beyond LEO, the possibility of satellite collisions is expected to grow significantly. This will force CubeSats to start implementing more radiation-hardening techniques, which, on pico- and nano-satellites, mainly consists of COTS components screening, radiation tests and real-time operation monitoring. This opens the need for CubeSat TID sensors, which are currently not available on the market.

In this thesis, the design of an absorbed dose sensor is presented. The thesis aims at presenting design requirements and solutions, along with simulations and preliminary tests. The presented sensor is planned to be flown on-board PW-Sat2 student satellite, in Q4 2017.

Brief description of thesis chapters:

- Abbreviations, conventions - present abbreviations and conventions used within this thesis,
- Introduction - this chapter, description of the thesis aims,
- Principles - introduces reader to radiation related problems and explains the theory of operation,
- Requirements - presents design requirements for this particular sensor, because it is designed specifically for PW-Sat2 satellite,
- Sensor design - presents high-level sensor design phase, explaining its operation on block and system level,
- Engineering model - describes the sensor model developed during this thesis, its design and simulations,
- Tests - presents results of conducted sensor tests,
- Future work - briefly describes the required next steps until flight solution is ready,
- Summary - summarizes thesis, work and outcome.

3. Principles

This chapter describes basic informations about radiation environment, failure modes in electronic devices and introduction to RadFET dosimetry.

3.1. Radiation on Low Earth Orbit

Radiation on LEO comes from trapped particle belts, solar particle events and cosmic rays [1]. There are also other sources of radiation, but they are negligible comparing to those effects.

Trapped particles

Electrons and protons are trapped in Earth's magnetic field, following magnetic field lines. They are a serious concern on Low Earth Orbit along polar regions and inside the South Atlantic Anomaly. In the figure the 3.1 radiation pattern along Earth is shown.

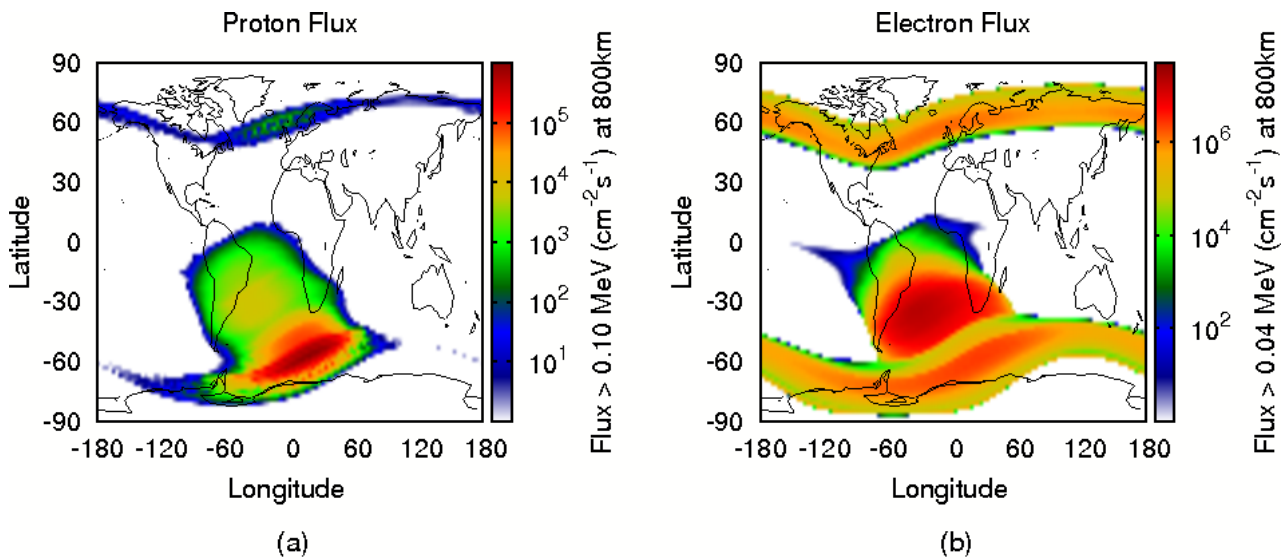


Figure 3.1: Radiation pattern on LEO. Source: [1]

Solar flares

During solar flares large fluxes of protons are produced, and some of these reach Earth. Earth's magnetic field provides some shielding from them, but they may become trapped inside, easily reaching polar regions and South Atlantic Anomaly. Solar flares are unpredictable and represent a threat to spacecraft operations.

Cosmic rays

Cosmic rays originate from outside the Solar System. They are very high energy particles, making effective shielding very difficult. Flux of this kind of particle is low, therefore they mostly contribute to single-event processes.

3.2. Radiation effects on electronic devices

There are two basic effects of radiation on silicon components:

- ionizing effect
- displacement damage

These two effect are responsible for changing the parameters of semiconductor devices, which after some time can lead to failure of the device. The main source of this radiation are gamma (ionization) and neutron particles (displacement).

In space electronics during analysis and design two major problems are considered - Single Event Effects (SEE) and Total Ionizing Dose (TID). Every silicon and silica device is susceptible to both of those - and both have to be considered during product design, development and testing.

3.2.1. Single Event Effects

Single Event Effects are connected with the generation of electron-hole pairs in semiconductor material when exposed to ionizing radiation. The number of pairs generated is proportional to the energy deposited. For semiconductor devices, the parameter LET_{th} (Linear Energy Transfer Threshold) is defined, being a measure of how susceptible the device is. For particles with Linear Energy Transfer (LET - normalized particle energy per mass of the absorbing material) below this threshold no effect will be observed.

Single Event Effects are divided into two groups - non-destructive (fully recoverable, possibly after power cycle) and destructive (permanent damage) effects. These are described below, defined as in [14].

Non-destructive effects

- **Single Event Upset** - especially vulnerable are memory-based devices (like microprocessors, memories, Field Programmable Gate Array - FPGA etc). This phenomenon may alter the state of cells in memory - causing memory corruption. This can lead to complete device failure if not corrected.
- **Single Event Functional Interrupt** - subset of SEU - this effect causes the system to latch in a non-recoverable state (e.g. by switching to wrong state in state machine). The only option is to reset the circuit to back to a known state.
- **Single Event Transient** - are formed as spurious voltage/current pulses generated by the charge induced by striking particles. This can cause a variety of problems - from the disturbing of analog electronics to the anomalous switching of digital circuits. This effect strongly depends on the size of the feature in silica.

Destructive effects

- **Single Event Latch-up** - particle striking can cause the activation of a parasitic thyristor in the CMOS structure. This will lead to effectively shorting the voltage supply to ground, causing overheat and damage to the device.
- **Single Event Gate Rupture** - high energy particles coming through the thin gate (especially in MOS transistors) can cause generation of electron-hole pairs in gate and substrate - causing a high electric field across the gate. When this effect is strong enough it can cause permanent damage to the transistor.
- **Single Event Burnout** - an ion that traverses the transistor structure (through the source) can induce a current flow that turns on the parasitic npn transistor. This leads to effective short circuiting and damage to the device.

Mitigation techniques

Below recommended mitigation techniques for SEE are listed:

- SEU - redundancy, memory scrubbing,
- SEFI - watchdog, proper reset sequence,
- SET - use lower-integration scale devices, implement protection resistors etc.
- SEL - implement overcurrent circuits (like Latch-up Current Limiters),
- SEGR, SEB - use higher LET_{th} devices

3.2.2. Total Ionizing Dose

TID is defined as the total energy absorbed during exposure. This can be caused by any kind of radiation, behaving differently in every semiconductor device. In general, TID successively degrades electronic device parameters over time, causing them to stop functioning when critical irradiation is reached. The effect in p-MOSFET transistors is described in section 3.5.1.

3.3. Need for TID radiation dosimetry

During spacecraft missions, accumulated radiation levels should be monitored in order not to exceed certain guaranteed values for components. For example, near the end of its lifetime, a spacecraft can be commanded to deorbit into the atmosphere or move to graveyard orbit - before failure can occur, causing loss of control of the spacecraft, like, for example in Telstar-1. Absorbed dose simulation is a good method of its estimation, but, because radiation flux varies (due to cosmic events like solar flares), errors can accumulate during a satellite's lifetime. Flying by the South Atlantic Anomaly or Van Allen belts can cause inaccuracies in radiation estimations, so nearly all spacecraft implement sensors which constantly monitor the radiation levels absorbed by their electronics.

3.4. On-line TID radiation dosimetry

A number of possible dosimetry methods were considered:

- PIN diode - forward voltage shift during irradiation [31],
- memory dosimetry - single events cause bit flips in memory - accumulated number of errors reflects absorbed dose [27],
- FGMOSFET - change in differential channel current - indicative of radiation dose [5],
- RadFET - shift of threshold voltage of p-MOS transistor indicates irradiation [27].

Detailed description of those dosimetry methods can be found in [27].

For this sensor, it was decided to use RadFET as a sensing element. These kinds of sensor have already flown on many satellites and are used in medical and industrial dosimetry.

The most important advantages of RadFET dosimetry:

- sensor can be completely shut down during irradiation (no power consumption and increased reliability),
- integrated measurement (especially important for small dose rates),

- on-line, non-destructive readout,
- small size,

And the most crucial drawbacks:

- low sensitivity - requires sophisticated measurement setup,
- required temperature compensation.

3.5. RadFET Theory

The basic idea of RadFET, using metal-oxide semiconductor field-effect transistors (MOSFET), is to measure the threshold voltage shift, ΔV_{TH} and convert it into an absorbed dose.

3.5.1. Radiation effects on MOS transistors

Irradiation of MOSFET transistor results in threshold voltage shift. This is caused by trapping of holes (generated during particle strike) and creation of interface states on gate/bulk boundary. Those effects are shown in the figure 3.2.

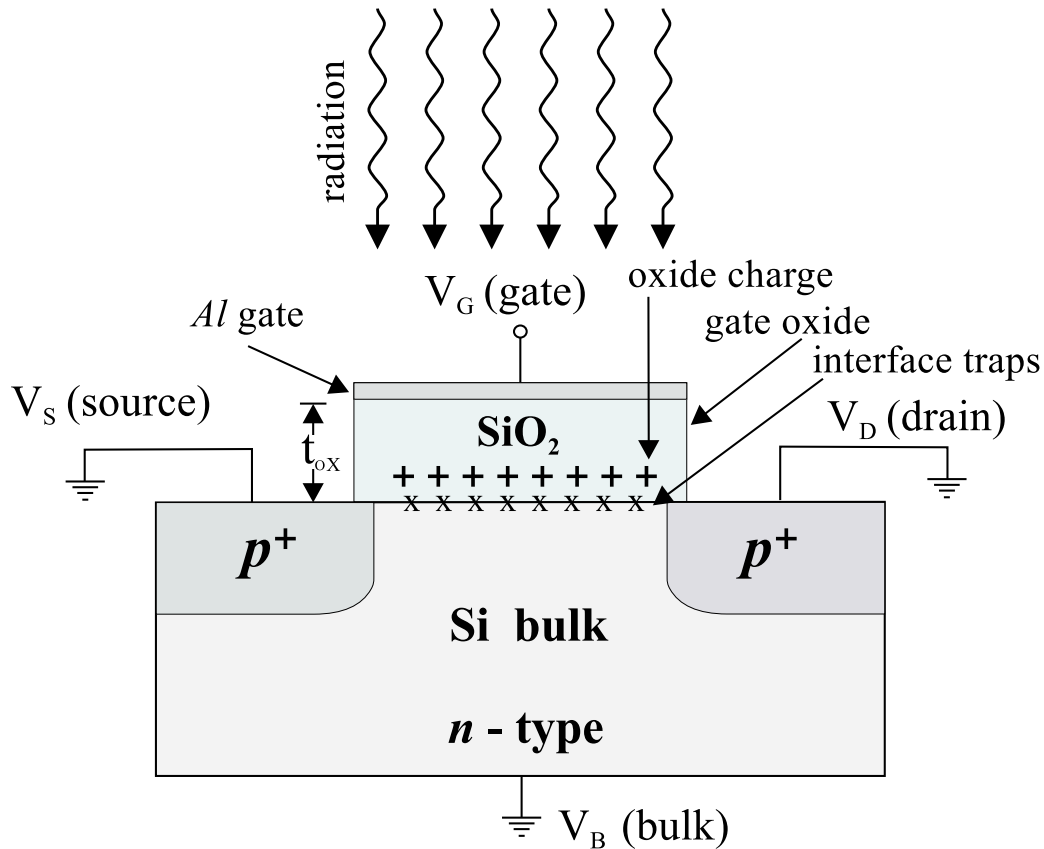


Figure 3.2: pMOS irradiation schematic. Source: [36]

Threshold voltage will shift according to the following equation [36]:

$$\Delta V_{TH} = A \cdot D^n$$

Where:

- ΔV_{TH} - threshold voltage shift
- A - constant
- D - absorbed dose
- n - degree of linearity (ideally $n = 1$)

3.5.2. Threshold voltage measurement

The simplest method to measure threshold voltage shift is to use diode configuration of MOS transistor, current source and measure voltage across, as shown in the figure 3.3.

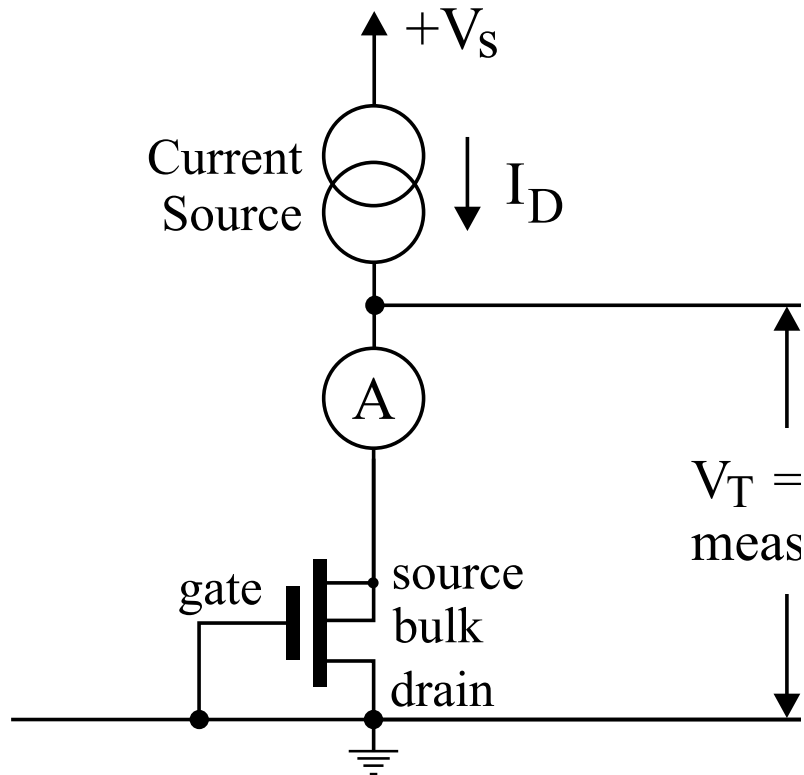


Figure 3.3: Measurement setup. Source: [36]

3.5.3. Temperature dependencies

Threshold voltage of transistor strongly depends on die temperature [45].

This dependency is usually described to be linear:

$$\Delta V_{TH} = A \cdot \Delta T$$

Where:

ΔV_{TH} - threshold voltage shift

A - constant

ΔT - temperature change

Constant coefficient depends on particular MOSFET, technology and (very weakly) irradiation. Usually this coefficient is in the range -0.1 to -1 mV/K.

In fact, nature of this dependency is non-linear [45], and higher-order approximation could be needed especially when better accuracy is necessary.

4. Design requirements

In this chapter the requirements for the TID sensor will be presented.

The finalised sensor is to be flown on-board the PW-Sat2 CubeSat satellite. Therefore, it should be designed for these particular requirements. In addition, it should be designed with active space standard and launcher requirements in mind. Additional requirements come from CubeSat Design Specification, which summarizes them for CubeSat type satellite [8].

4.1. PW-Sat2

The presented sensor is scheduled to be launched on the PW-Sat2 satellite [43]. Therefore it should be designed especially for this particular type of mission. In this section the PW-Sat2 mission will be presented.

PW-Sat2 is scheduled to be launched on Falcon9 rocket from SpaceX company in Q4 2017.



Figure 4.1: Falcon9 rocket. Source: [37]

In the figure 4.2 an exploded render of PW-Sat2 is presented.



Figure 4.2: PW-Sat2 render. Source: [44]

4.1.1. Primary mission

The primary mission of PW-Sat2 is to test the deorbit sail. When satellite mission ends, it has to be safely deorbited (or moved to graveyard orbit). Due to new regulations, satellite has to be removed from the LEO region no later than 25 years after the end of vehicle operations [23]. Purpose of deorbit sail is, after satellite operations, to open and increase atmospheric drag, shortening satellite life and cause deorbitation. More information about this experiment can be found in [42].

A render of PW-Sat2 with opened sail is shown in the figure 4.3.

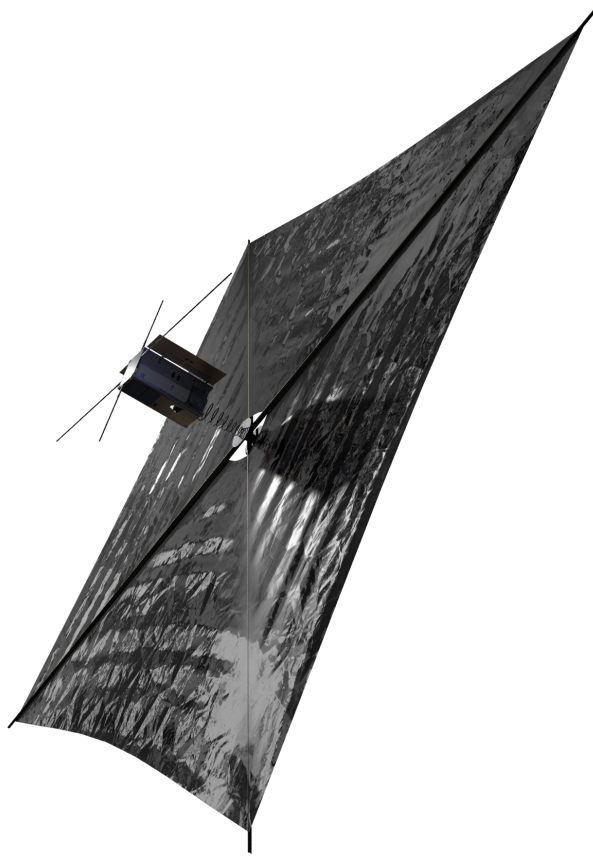


Figure 4.3: PW-Sat2 with opened sail. Source: [44]

4.1.2. Lifetime

Due to its primary mission, the basic lifetime of PW-Sat2 is planned to be 40 days long. After this time the deorbit sail will be opened and orbit will slowly decay. Deorbitation from nominal orbit is planned to take about one year [33], but possibly with an unreliable data connection. Therefore the sensor should be able to measure the dose absorbed during the primary mission (40 days), but also to work throughout the full predicted mission - about one year.

4.1.3. Orbit

PW-Sat2 is planned to be launched to a sun-synchronous circular orbit of attitude 575 km, with LTAN of 10:30 [33].

4.1.4. Radiation analysis

Simulations in SPENVIS [12] were performed to estimate TID accumulated during the PW-Sat2 mission. In the figure 4.4 dose as a function of shielding thickness was plotted, during year-long mission on predicted orbit.

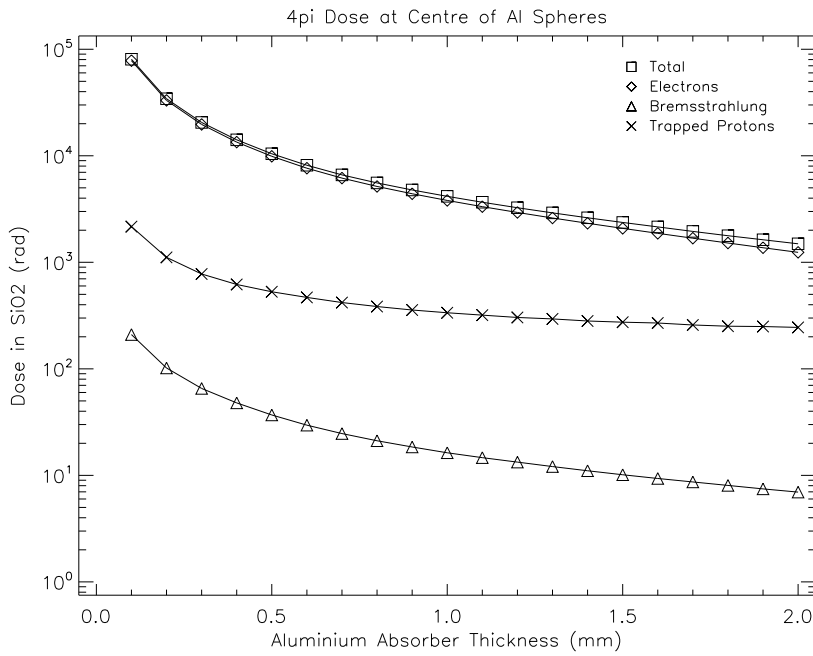


Figure 4.4: TID vs shielding during one year mission on 575 km orbit

The shielding of PW-Sat2 is about 0.5 mm thick (aluminum sides as well as aluminum substrate for solar cells - 4.2). Therefore, predicted dose during the primary mission is 1 krad and over the full, one year mission, is about 10 krad.

4.2. Sensor requirements

Summing PW-Sat2 mission analysis, high-level sensor requirements were estimated, summarized in the table 4.1.

Table 4.1: Sensor requirements

Requirement	Value
Range	10 krad
Resolution	10 rad
Total accuracy	± 100 rad

4.3. Applicable standards

The sensor should comply to ECSS [10] standards. They are required by the launch provider and describe good practice during space product development.

ESCIERS [11] provides valuable knowledge about component qualification, testing and verification.

4.4. Electrical requirements

The sensor will be placed on-board PW-Sat2. Therefore it should comply to its standards - power supplies, communication interfaces etc.

4.4.1. Electronics stack

Modules on PW-Sat2 are connected in the PC-104 stack structure as shown in the figure 4.5. It is placed inside the satellite housing and consists of (from the top):

- **Payload module (PLD)** - where the sensor will be located,
- On-Board Computer (OBC) - main data processing unit,
- Attitude Determination and Control Subsystem (ADCS) - controls attitude (detumbling and sun-pointing),
- Electrical Power System (EPS) - charges and discharges batteries, provides safety mechanisms,
- Battery module (ACC) - main energy storage,
- Communication transceiver (COMM) - VHF & UHF full duplex transceiver,
- Antennae module (ANT) - antennae for uplink and downlink.

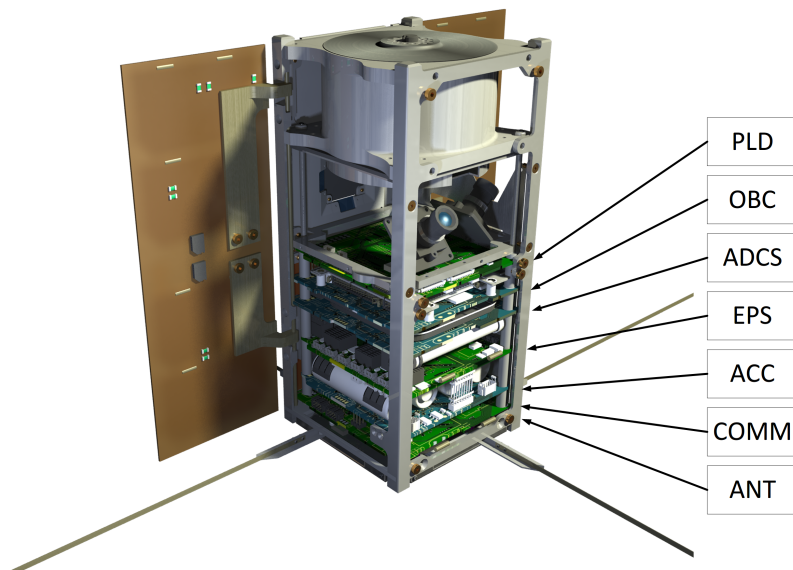


Figure 4.5: PW-Sat2 electronics stack

4.4.2. PC-104 connector

PLD board is connected to OBC with PC-104 connector. This connector provides data and power connections to the satellite bus.

The connector consists of:

- I^2C bus, connected directly to MCU on OBC,
- interrupt line on which the sensor can notify OBC about command completion,
- SENS 5 V line, powered only when sensor is commanded to be enabled.

4.4.3. Power rail

As mentioned earlier, the power for the sensor is +5 V, activated whenever the sensor is to be accessed by OBC.

The power line is controlled and protected by a Latchup-Current Limiter FPF2701MX placed on the EPS board. Therefore, additional latchup protection is not necessary in this design. However, this sensor will not be the only one on the PLD board and should have its own power switch. The PLD board is enabled and disabled by EPS on the OBC command and the sensor should be enabled only during TID readout. Having this in mind forces the design to be immune to immediate shutdowns and dose have to be accumulated off-line.

4.4.4. Power consumption

During irradiation sensor should be completely turned off. It decreases possibility of radiation damage and increases overall system reliability.

During readout the required power should be less than 1 W.

4.4.5. Data interface

The sensor is connected to the OBC via the I^2C interface. On this bus, OBC is the master, while the sensor is one of the slaves. The PLD board can be disabled and can therefore provide isolation of the I^2C bus when it is powered off.

4.4.6. Radiation immunity

The design should itself be immune to radiation. For PW-Sat2, a threshold of 10 krad was chosen for all COTS components. Semiconductors should have radiation tests as described in [16].

4.4.7. Electromagnetic compatibility

EMC requirements are described in [13]. This standard was tailored to PW-Sat2 because the power rail is 5 V, rather than the (28 V) featured on bigger spacecraft.

- Conducted susceptibility is shown in the figure 4.6 . It was created by down-scaling figure A-4 from [13] by factor of $28\text{ V}/5\text{ V} = 5.6$. The EMC limit on the power line is defined as a constant 175 mV from 30 Hz to 100 kHz. The sensor should be able to filter this ripple to produce stable power for analog devices. In addition, it should be taken into account that output DC-DC converters on EPS run at 500 kHz.

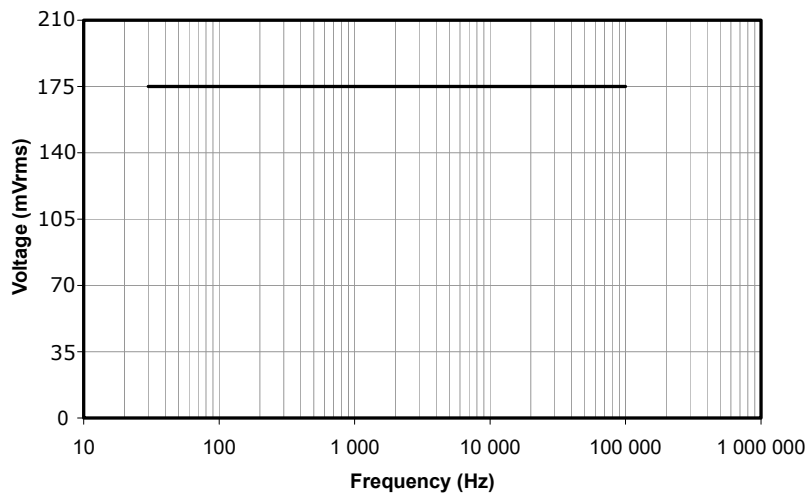


Figure 4.6: Conducted susceptibility limit, frequency domain. Source: [13]

- Conducted emission is defined in the figure 4.7.

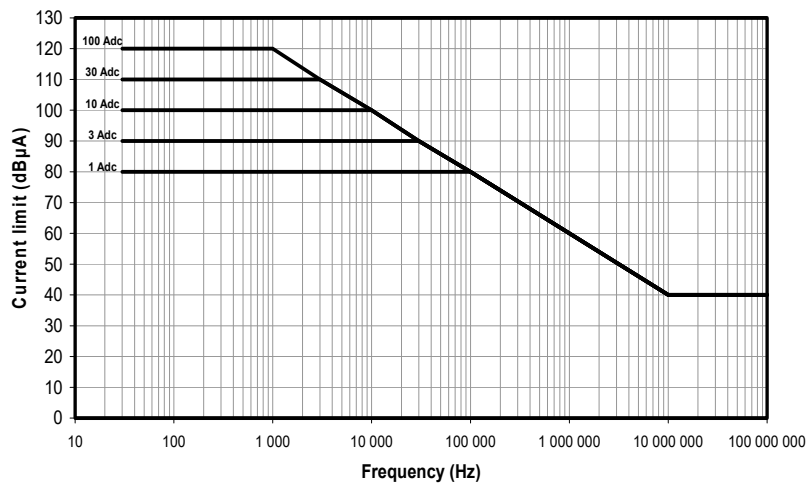


Figure 4.7: Conducted susceptibility limit, frequency domain. Source: [13]

- Radiated susceptibility. On board PW-Sat2 is a communication module transmitting 0.5 W of power at 435.02 MHz. It is planned that during readout, the radio transmitter will be disabled, but proper tests should be conducted to check for possible errors and faults.

PLD board is placed near OBC - so radiated emissions from digital lines can potentially couple to sensor elements causing noise and errors. Proper tests will be conducted and if necessary shielding will be implemented.

- Radiated emission. The sensor is not predicted to emit any kind of radio waves. In case of any detected anomalies, further design decisions would have to be made.

4.4.8. Inrush current

Inrush current has to be limited to maximum power consumption to not trigger LCL on EPS (0.5 A).

4.4.9. Reliability of components

This sensor is not a critical part of the satellite. Nonetheless, reliable components should be used to ensure proper results.

Every used component should have a failure rate of 0.1% or lower. This is essential in capacitors and other passive components.

4.5. Mechanical requirements

In this chapter design constraints and mechanical requirements of Falcon9 are presented. Launcher requirements were taken from [38].

4.5.1. PCB

PCB of PLD board is standard 4-layer FR4 board with stack shown in the figure 4.8. Its dimensions are shown in the figure 4.9. The sensor design must, of course, occupy only a small amount of space on the board. For the sensor footprint, the limits are 3 cm × 3 cm double sided.

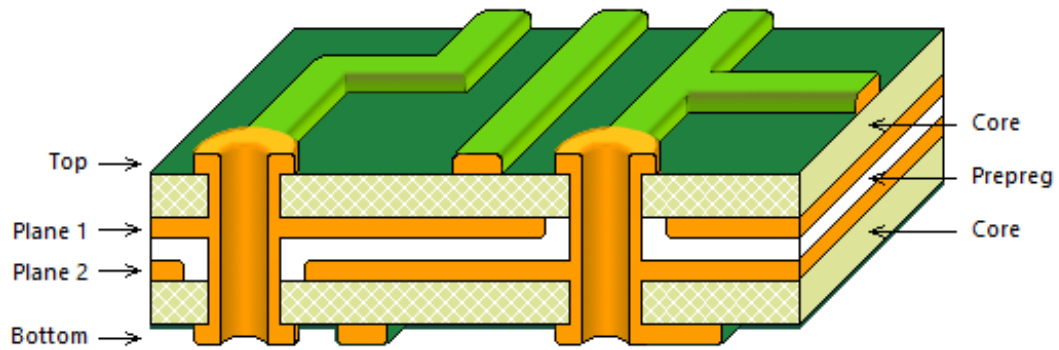


Figure 4.8: PLD board PCB stack

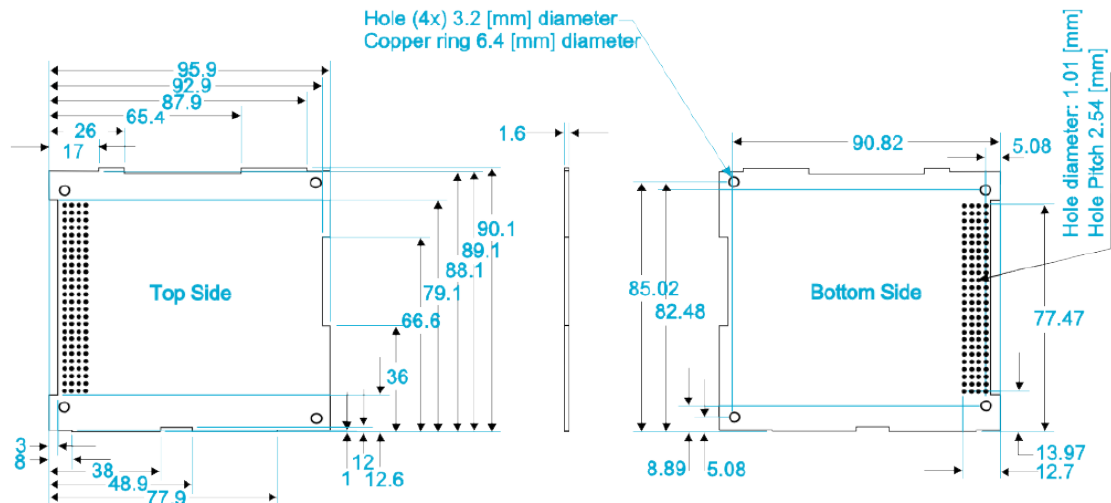


Figure 4.9: PC-104 size

4.5.2. Outgassing

Every component used should be able to work in vacuum. Outgassing of components should be known to conduct required vacuum tests before launch. Too great an outgassing coefficient can result in damage to the turbomolecular pump in the vacuum chamber.

4.5.3. Vibration

During the rocket launch, large vibrations occur on the payload, therefore the rocket payload should be immune to vibration. In the case of heavy electronic components, appropriate glue should be applied to prevent joint cracks.

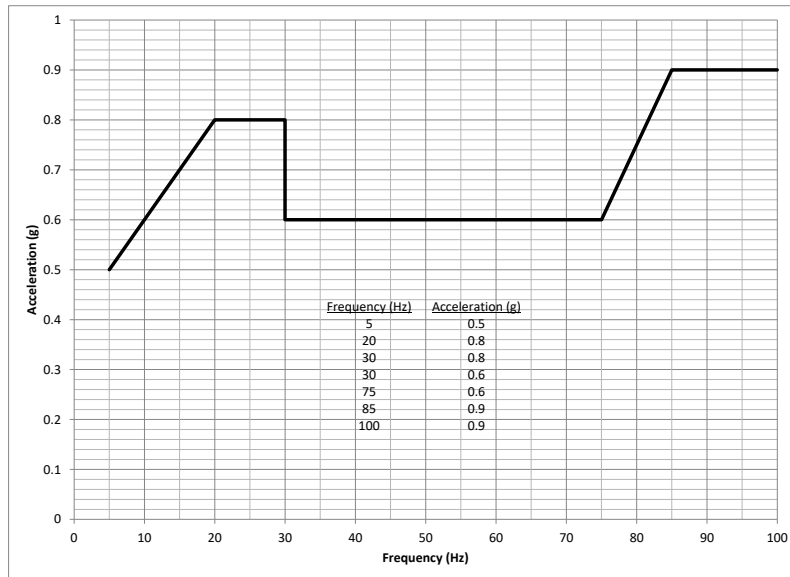


Figure 4.10: Falcon9 maximum axial equivalent sine environment. Source: [38]

4.5.4. Operation temperature

The sensor should work in every operational case a satellite can be. Simulations were performed to find the boundaries of the possible temperature range inside the satellite. In [34] results are presented.

For the PLD board, the operation range is 0 °C to 60 °C. If the measured temperature is outside this range, the sensor will not be enabled.

4.5.5. Thermal cycles

On the PW-Sat2 orbit, the sun illumination is changing every \approx 90 min. Therefore a large number of thermal cycles are applied to the On-Board electronics, which can cause joint cracks as well as component failures. Proper soldering and component selection will be made, according to ECSS.

As described in [15] the sensor should pass thermal cycle tests: 100 times from $-(100 \pm 5)^\circ\text{C}$ to $(100 \pm 5)^\circ\text{C}$ in a vacuum environment. This will be tested on Qualification Model.

5. Sensor design

This chapter will cover sensor basics, sensing element selection and theory of operation. The design will be presented at a system-level view. For a more detailed description of the electronics, please skip to chapter 6.

5.1. Review of commercially available RadFETs

Commercial solutions are based on a modified MOS structure (with thicker gate region). Example silicon structure is shown in the figure 5.1. Different companies produce their own RadFET devices, by designing individual structures fitted to particular requirements. Researched companies only produce the RadFET sensors, leaving the readout circuit design for the customer to realise. A physical schematic and description for RadFET sensors is found in section 3.5.1. In the table 5.1 commercially available RadFETs are compared.

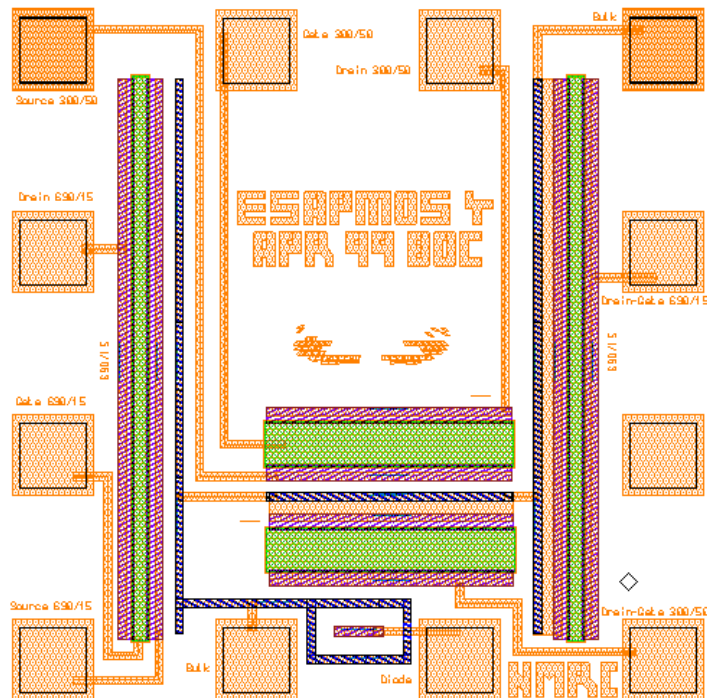
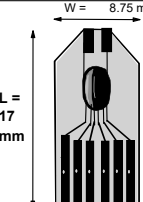
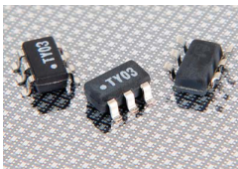
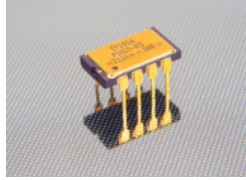


Figure 5.1: 4x RadFET silicon structure by Tyndall. Source: [22]

Table 5.1: Commercial RadFET comparison

Type:	REM RFT300	Tyndall TY1003	Tyndall TY1004
Image:			
Package:	custom	SOT23-6	8-pin ceramic DIL
# of transistors:	2	2	2
Recommended readout current:	10 - 500 μ A		10 μ A
TID dependency:	$n = 1$, $A = 0.117 \text{ mV/rad}$	$n = 0.46$, $A = 29.5 \text{ mV/rad}$	$n = 0.41$, $A = 65.6 \text{ mV/rad}$
Temperature readout:	diode	diode	diode

5.2. COTS MOSFET as RadFET

RadFETs are specifically designed MOSFETs that act as radiation sensors. However, the parameters of COTS MOSFET transistors also depend on total absorbed dose. They are much cheaper, but require proper calibration and testing in order to be considered as a flight solution.

Many articles and papers prove that COTS MOSFETs can be used reliably as TID sensors. A number of available transistors were tested, their basic characteristics are compared in the table 5.2. Parameters are taken at unbiased gate.

Table 5.2: COTS MOSFET comparison

Type:	3N163	ZVP3306	ZVP4525	BS250F	CD4007
Reference:	[9]	[28]	[28]	[28]	[28]
Package:	TO-72	TO-92	SOT-223	SOT-23	TSSOP-14
$I_{ZTC} [\mu\text{A}]$:	225	-	-	-	145
Sensitivity [mV/Gy]:	24.3 ± 1.8	3.7 ± 0.3	3.4 ± 0.4	3.1 ± 0.4	4.6 ± 0.1
$V_{TH_0} [\text{V}]$:	$2.0 - 3.0$	$2.0 - 3.0$	$1.5 - 2.5$	$2.5 - 3.5$	$1.9 - 2.5$
$V_{TH} @ 100 \text{ Gy} [\text{V}]$:	5.61	3.4	2.88	3.85	2.97

3N163 type have the greatest sensitivity - but bearing in mind the 5 V supply for the sensor, it was discarded for too small range. The second best type is CD4007, which was selected for testing. Its parameters are suitable for the use under discussion, as shown in the table 5.3.

Other advantages of CD4007 are:

- 3 P-MOS in one package - averaging/redundancy,
- additional diodes and transistors in device - possible temperature measurement
- small, vibration and thermally resistant package

5.3. Selected MOSFET - CD4007

The CD4007 consists of three complementary pairs of N- and P-channel enhancement mode MOS transistors. Internal connection diagram is shown below in the figure 5.2. Predicted parameters of those transistors are collected in the table 5.3.

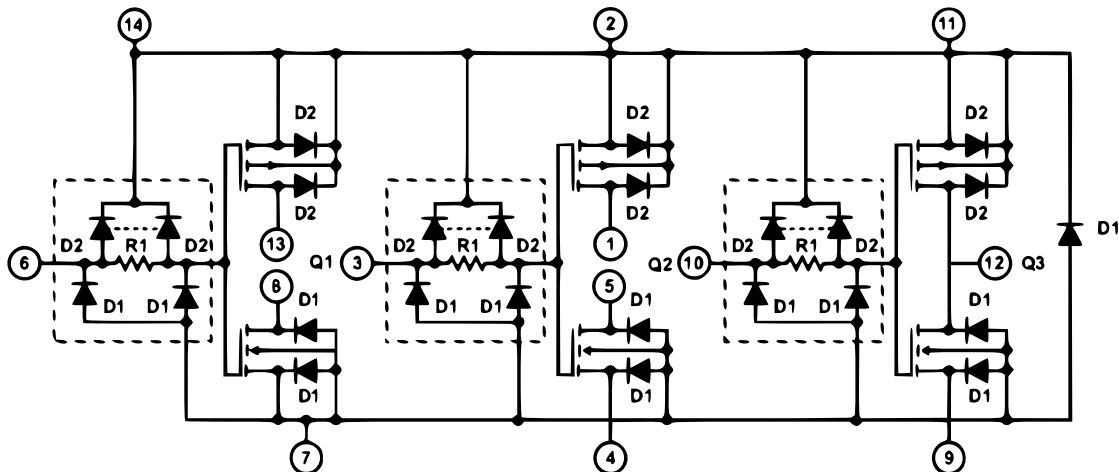


Figure 5.2: CD4007 internal diagram. Source: [4]

Table 5.3: CD4007 parameters

Transistor type:	3x P-MOS and 3x N-MOS
Supply voltage:	3-18 V
Threshold voltage:	1.8 V @ 100 μ A
Temperature range:	-55 °C - 125 °C
Zero-temperature coefficient current:	140 μ A
Predicted sensitivity:	4.6 mV/Gy

5.4. Threshold voltage measurement

Threshold voltage changes with TID accumulated. The easiest method to measure change of this parameter is to connect the MOSFET in diode configuration, forcing constant drain current. A block diagram of this method is shown in the figure 5.3.

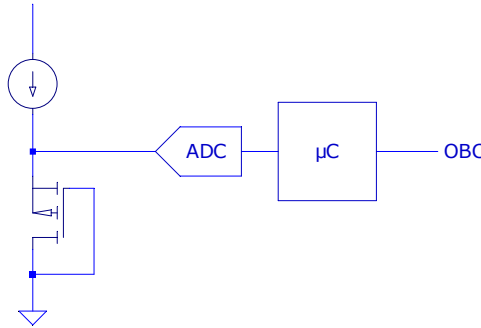


Figure 5.3: Threshold voltage readout block diagram

In saturation region, drain current is described by the following equation (body effect is negligible):

$$I_D = A \cdot (V_{GS} - V_{th})^2$$

Where:

- | | |
|--|--------------------------------------|
| I_D | - drain current |
| $A = \frac{\mu_n C_{ox}}{2} \frac{W}{L}$ | - constant for particular transistor |
| V_{GS} | - gate-source voltage |
| V_{th} | - threshold voltage |

Because only the threshold voltage change is of interest, measuring V_{GS} has the same effect:

$$I_D = A \cdot (V_{GS_1} - V_{th_1})^2 = A \cdot (V_{GS_2} - V_{th_2})^2$$

$$\Delta V_{GS} = \Delta V_{th}$$

The sensor should be shut down during irradiation - therefore no-bias method was used. It allows for complete isolation of supply power to the sensor, enabling it only for readout.

5.5. Temperature measurement

Because threshold voltage strongly depends on die temperature, this effect has to be compensated for. The flight MOSFET will be calibrated in a thermal chamber prior to launch, thus obtaining characteristic curves.

A number of possible temperature measurement techniques were considered during this thesis:

Table 5.4: Temperature readout methods

Method	Pros	Cons
PT-1000 sensor glued to MOSFET	accurate reading	large thermal resistance, difficult assembly, low reliability
ESD diode measurement in CD4007	no additional sensor	complicated current, multiplexing circuit, unknown characteristics
body diode in N-MOSFET in CD4007	simple setup, reliable, known characteristics, low thermal resistance	no possibility of simultaneous readout of threshold and temperature (short thermal lag)

The chosen solution: to measure temperature of silicon die using body diode in complementary N-MOS transistor. A block diagram of this proposed solution is presented in the figure 5.4.

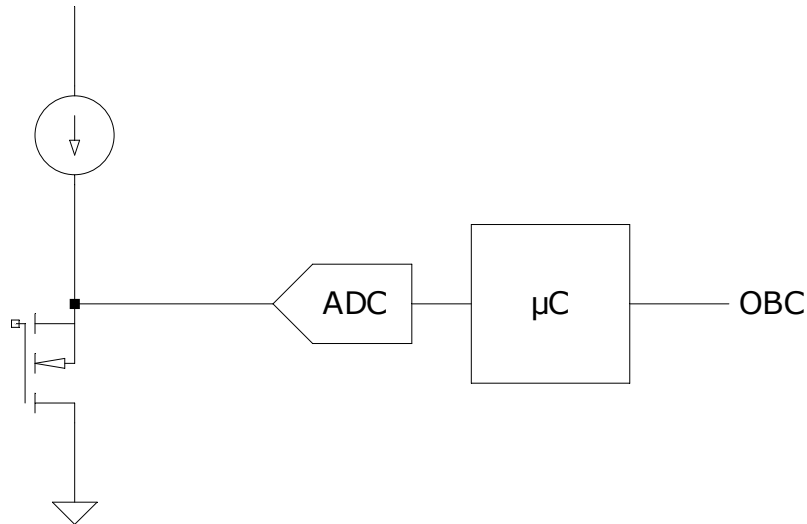


Figure 5.4: Temperature measurement block diagram

During calibration, both the temperature characteristics of the diode and the p-MOS threshold voltage will be obtained. They will be used to compensate for the threshold voltage shift associated with temperature. An individual flight component will be placed in a thermal chamber, and a proper look-up table will be created, with possible polynomial approximation.

5.6. Characteristic curves

During M. Gumiela's thesis, [18] a calibration stand for CD4007 was developed. As an outcome of that project, rough calibration curves were obtained, which are presented below.

p-MOSFET transfer characteristics

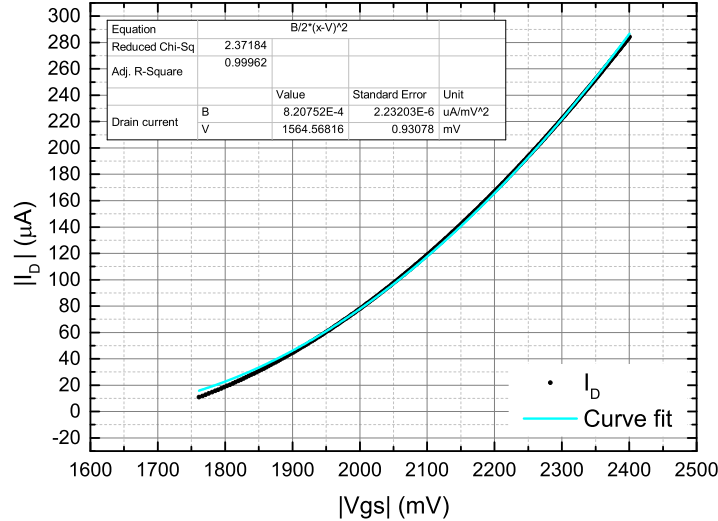


Figure 5.5: CD4007 p-MOSFET transfer characteristics. Source: [18]

Linearized temperature coefficient of threshold voltage

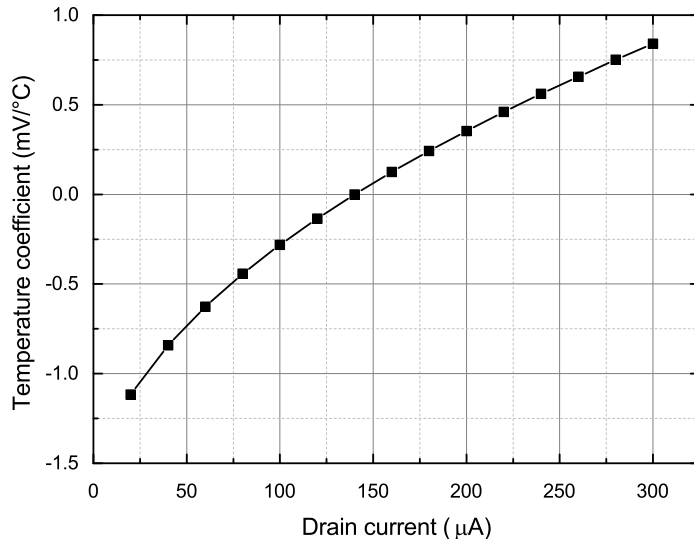


Figure 5.6: Linearized temperature coefficient of threshold voltage. Source: [18]

Body diode forward voltage temperature calibration

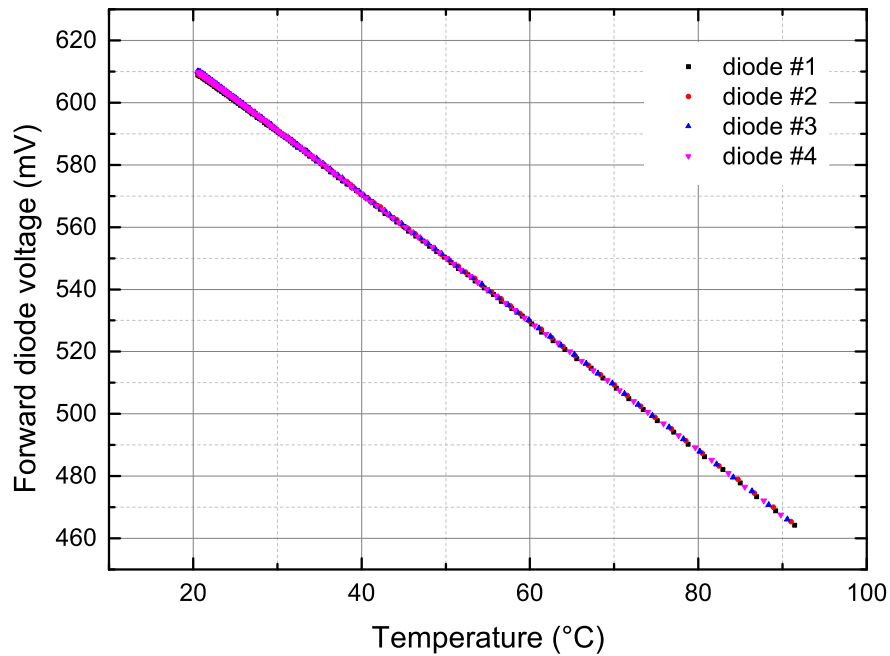


Figure 5.7: Body diode temperature calibration. Source: [18]

5.7. Operating point selection

A current source value had to be chosen, keeping in mind the requirements and working conditions.

In theory, a zero-temperature coefficient current would be optimal, but after irradiation it could shift slightly, causing a significant error. Additionally, due to limited availability of elements on the market and slight differences between devices, this operating point would be very difficult to achieve.

As a tradeoff between low temperature coefficient and low starting threshold voltage, (to increase sensor range) the current value of $125\ \mu\text{A}$ was chosen.

6. Engineering model

This chapter will describe the engineering model developed during this thesis.

The model should be as close to the flight model as possible - although it was, in fact, developed on a different factor board.

The model was developed as a flight-ready version for sensor calibration and testing alongside flight software developing and testing.

6.1. Background - calibration stand

During development of the sensor, the previous model was developed to test and calibrate MOSFET transistors for use as radiation dosimeters. The calibration stand was developed by M. Gumiela in his thesis [18]. The basic goal was to develop a measurement device which can be used to determine the final operational point, calibrate the radiation response and perform temperature calibration of the flight sensor.

The test and calibration stand allows for the carrying out of simultaneous investigations of parameters of multiple MOSFETs (i.e. 18) and diodes (i.e. 6). It is possible to obtain the transfer characteristics of the DUT (I-V) utilizing an adjustable constant current source, thermal calibration ($V_{th}(T)$, $V_d(T)$) thanks to precise reference thermometers, Iztc investigation and finally TID on-line calibration.

6.2. Block diagram

Block diagram of the proposed system based on CD4007 is presented in the figure 6.1.

It was designed with miniaturization of the sensor in mind - to fit on PW-Sat2 PLD board. Because CD4007 has 3 complementary MOS pairs it was proposed to use 3 p-MOS transistors as TID sensors - to improve the fidelity of the measurements. One n-MOS is used as a temperature sensor. Current source and ADC are multiplexed between 4 channels - this reduces board footprint and increases sensor reliability and accuracy. With readout fidelity in mind, a 3-wire method on the multiplexer was implemented.

The system consists of few basic building blocks, each of them will be detailed in this chapter:

- 125 μ A constant current source,
- CD4007 sensing element (3x p-MOS & 1x n-MOS),
- differential ADC,
- multiplexer

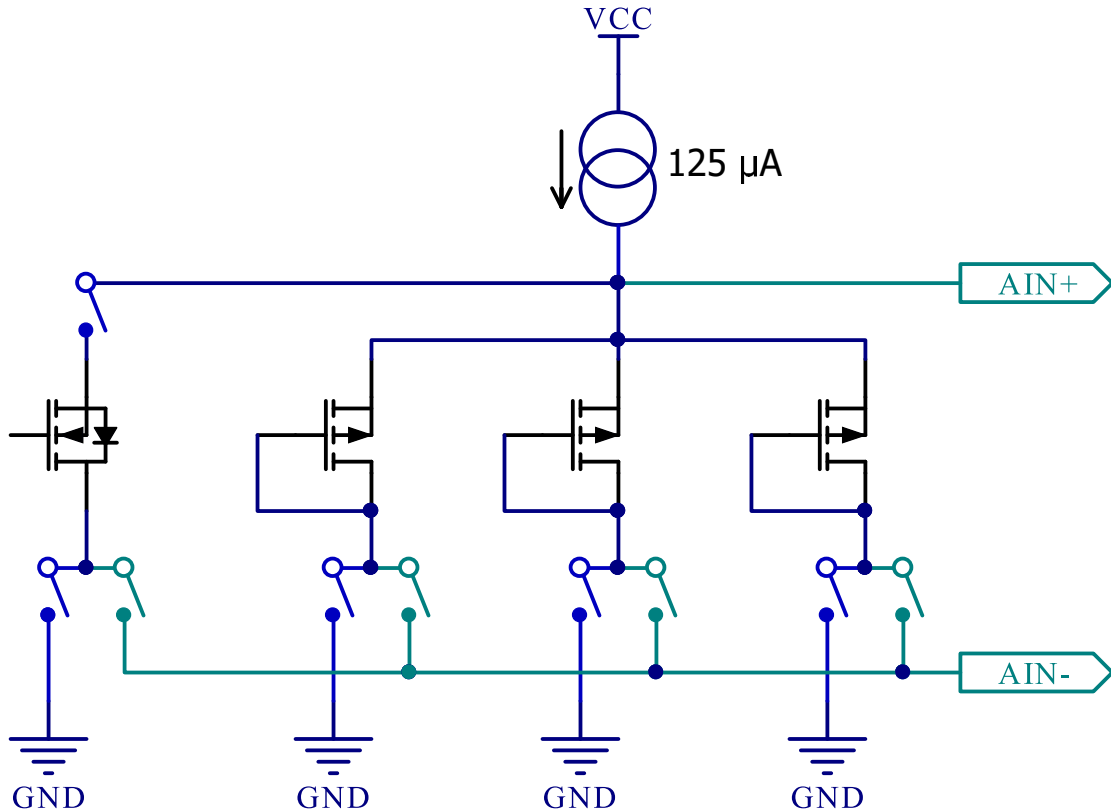


Figure 6.1: Block diagram

6.3. Low-level requirements

Using design requirements and characteristic curves from 5.6 low-level specifications were listed:

- operating temperature range: 0 \div 60°C,
- compensated threshold voltage stability: ± 0.5 mV,
- current source value: $125 \mu\text{A} \pm 50 \text{nA}$,
- ADC resolution: 0.1 mV @ 5 V reference = 16 bit

6.4. Analog front-end

In this section decision and schematic diagrams of building blocks are presented.

6.4.1. SPICE models

Design should be validated by simulation. In this thesis, LTSpice XVII was used.

Models used during simulation:

- CD4007 - model RIT4007P7 from Rochester Institute of Technology [17],
- Linear Technology components are embedded in LTSpice,
- other devices were modelled by hand using datasheets

6.4.2. Linear regulator

Positive rail +5 V on PC-104 stack comes from EPS, more specifically, this voltage is generated by a DC-DC converter (with 500 kHz switching frequency). Because of low noise requirements, the analog supply voltage has to be very well regulated and filtered. Because V_{TH} of transistor will increase with absorbed dose, dropout from 5 V should be as low as possible. As a tradeoff between this requirement and the available solutions on the market, analog rail voltage was chosen to be 4.7 V.

As an LDO regulator LT3042 was selected. It is ultralow noise, ultrahigh PSRR RF linear regulator by Linear Technology. Key specs [26]:

- ultralow noise 0.8 μ VRMS (10 Hz to 100 kHz),
- output current 200 mA
- input range 1.8 V to 20 V, output range 0 V to 15 V
- ultrahigh PSRR 79 dB at 500 kHz, more detailed graph is shown in the figure 6.2.
- low dropout voltage of 200 mV

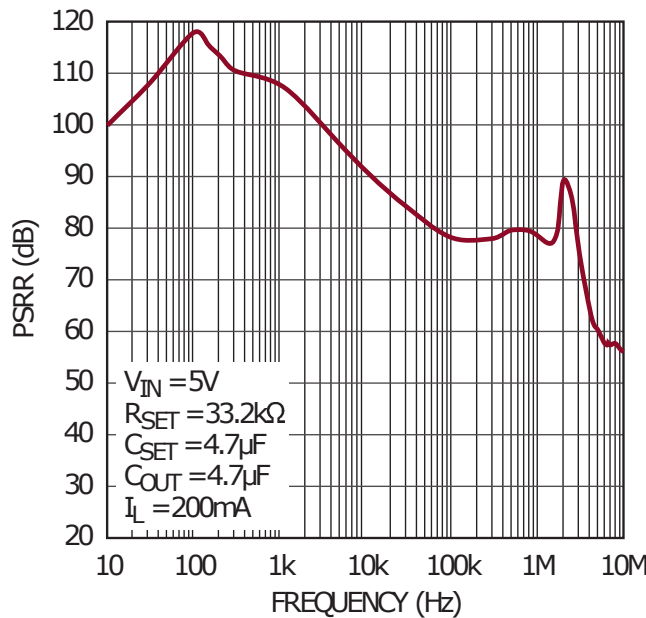


Figure 6.2: LT3042 PSRR. Source: [26]

Thanks to this regulator, the conducted susceptibility requirement was met (175 mV input ripple is cut down to 19 μ V, which is enough for ADC to filter).

6.4.3. RadFET power switch

Because the main PLD microcontroller is also controlling the other sensors (photodiodes, temperature sensors), the RadFET analog front-end has to have the possibility to be turned off. For this purpose, the TPS2551DBVx current-limited power-distribution switch was implemented in the design.

More accurately, two of them were implemented - one to disable the digital part of ADC and the second to disable all analog parts of the design.

Apart from possibility of isolating the RadFET they provide point-of-load latch-up current limitation, allowing an ability to cut down the power in case of SEE even faster.

6.4.4. Current source

The current source has to be the most accurate part of the design, because the measured voltage depends on the square of its variation. It was assumed that 50 nA current stability across temperature and aging range would be sufficient. The current source has to supply both the MOSFET (static resistance at operating point of about $20 - 25 k\Omega$) and the body diode temperature sensor (static resistance at operating point of about $3 - 7 k\Omega$).

The main concept of the current source is based on the Burr-Brown application note [7]. The idea schematic is shown in the figure 6.3.

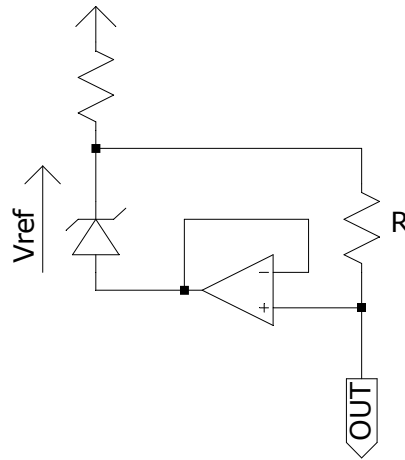


Figure 6.3: Current source block diagram

Output current is set by shunt voltage reference and resistor R , given by equation:

$$I_{OUT} = V_{ref}/R$$

Therefore, stability of output current depends on reference voltage and resistor accuracy.

Shunt reference

After irradiation MOSFET V_{DS} is planned to be no more than 2.5 V, so the reference voltage has to be lower than 2 V.

Linear Technology LT1634-1.25 shunt voltage reference was chosen. It is one of the best shunt references from Linear Technology. Basic specification [25]:

- 0.05 % initial accuracy,
- 10 ppm/ $^{\circ}\text{C}$ maximum temperature drift,
- $< 1 \Omega$ dynamic resistance,
- $10 \mu\text{A}$ minimal regulation current

Shunt resistance was chosen to make minimal current flowing through shunt reference large enough for specified loads - final value of $5 \text{ k}\Omega$.

Series resistor

The value of this resistor reflects the required current flowing through the MOSFET. The nominal value selected was $10 \text{ k}\Omega$.

The stability of this resistor across a temperature range is critical because it directly changes output current. To achieve the specified requirement, a $10 \text{ k}\Omega / 5 \text{ ppm}$ resistor was chosen (APC0603T10K0Z).

The manufacturer does not specify the exact value and profile of the temperature coefficient - so both worst cases were simulated (-5 ppm and 5 ppm).

Operational amplifier

The operational amplifier in this circuit should have very low bandwidth (noise limitation), low offset voltage (precision) and a small footprint. LTC2054 was selected - key characteristics:

- $3 \mu\text{V}$ offset voltage,
- common mode $\pm 0.5 \text{ V}$ input/output range,
- 500 kHz gain-bandwidth product,
- device in Military Plastic package (temperature range $-55 \div 150^\circ\text{C}$)

Simulation

Behavioral simulations were performed to find all possible problems with the circuit:

- temperature dependency,
- output resistance range,
- noise and stability

MOSFET/diode was replaced by a resistor emulating its static resistance ($2 \text{ V}/125 \mu\text{A} = 16 \text{ k}\Omega$, $0.6 \text{ V}/125 \mu\text{A} = 5 \text{ k}\Omega$, respectively). Simulation view is shown in the figure 6.4.

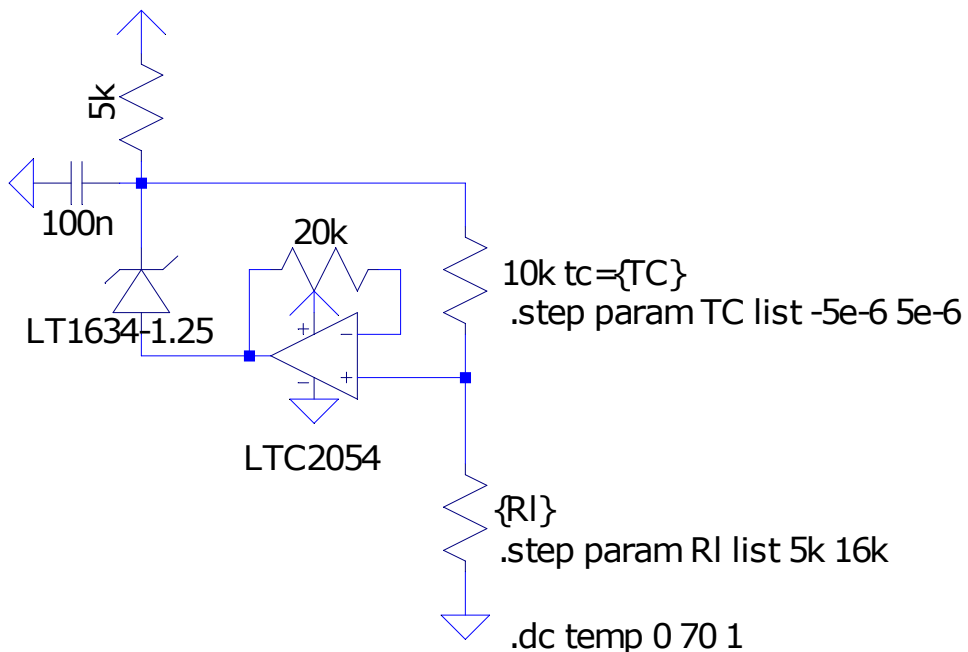


Figure 6.4: Current source simulation

Temperature dependency

Output current is shown in the figure 6.5, simulation was performed on two different loads and resistor temperature coefficients.

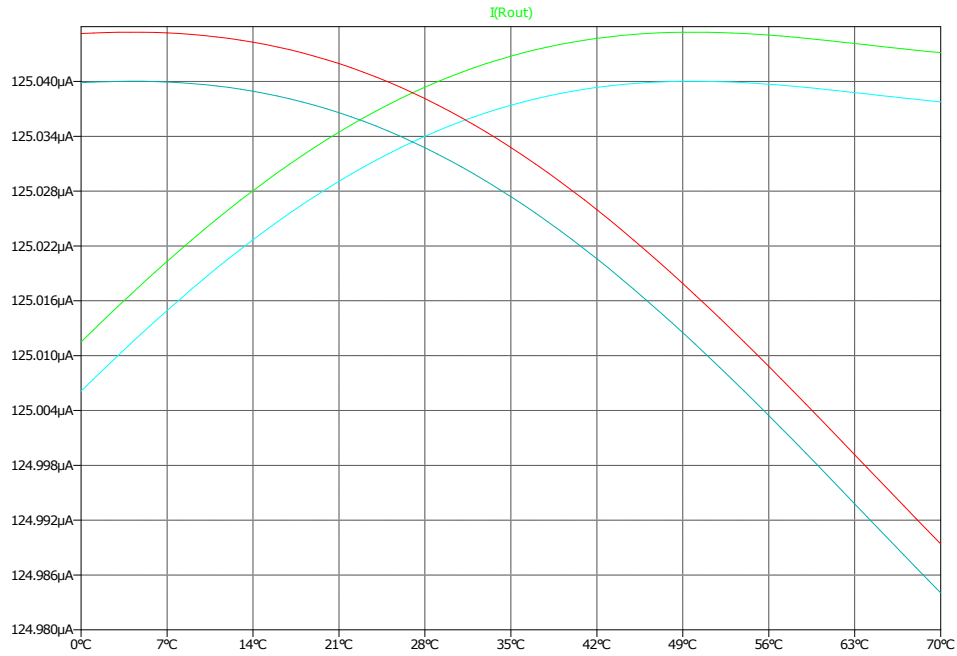


Figure 6.5: Current source simulation result - output current

Taking worst-case scenario, output current change across temperature range does not exceed 50 nA.

Output resistance range

Simulation shows that current source works reliably between $1400\ \Omega$ and $22.5\ k\Omega$. More detailed graph is shown in the figure 7.3.

6.4.5. Analog to digital converter

The analog to digital converter is responsible for reading V_{DS} voltage across the transistor and voltage across the diode. Due to very low changes, high accuracy and resolution is required. Additionally, complex mixed signal elements like ADC should be radiation tested to prove long term reliability. To achieve at least 0.1 mV resolution, ADC has to be at least 16 bits.

Due to constraints on the system and reliability issues, the AD7714 from Analog Devices was chosen. Radiation tests have shown that it fails between 10 krad and 20 krad, with no degradation up to 10 krad [21].

Internal diagram is shown in the figure 6.6. Key specs:

- 24 bits,
- 0.0015 % nonlinearity,
- programmable gain (1 ÷ 128),
- 3 fully differential or 5 pseudo-differential input channels
- 3 V or 5 V operation
- separated digital and analog supply and grounds,
- SPI interface
- 0.25 Hz sampling frequency for strongest filter,

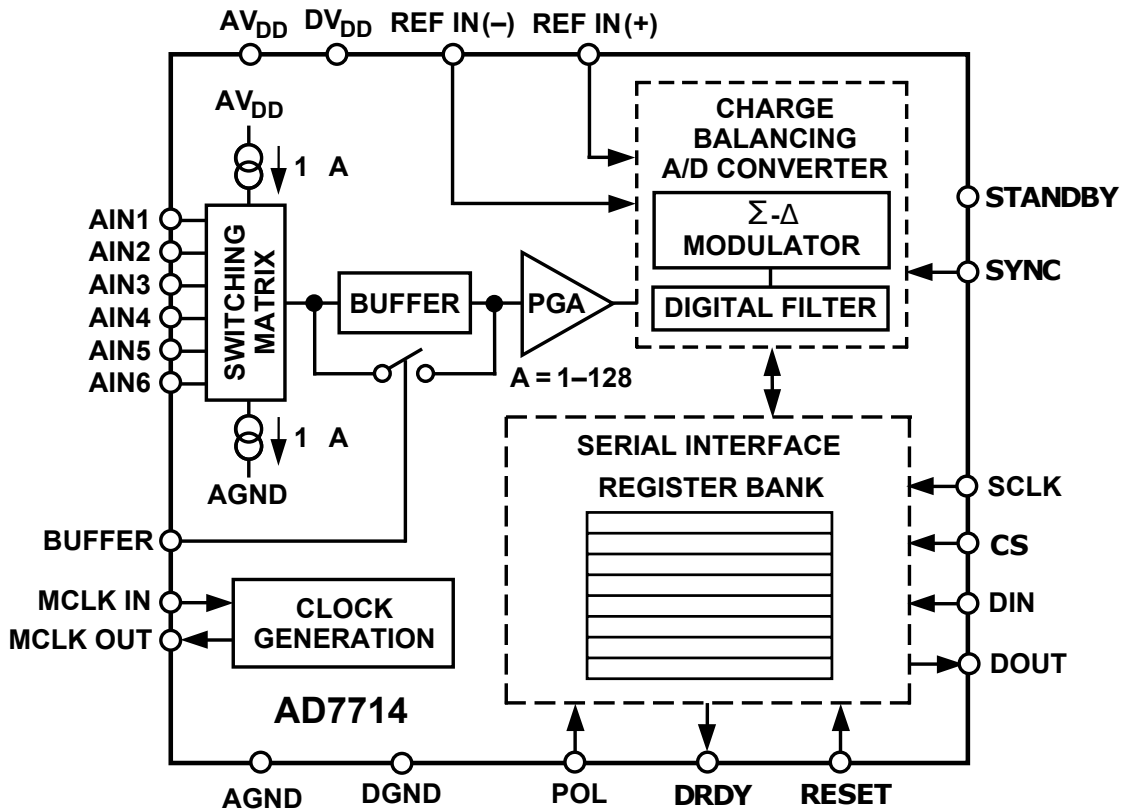


Figure 6.6: AD7714 internal block diagram. Source: [2]

AD7714 requires external crystal or clock oscillator in the frequency range 1 MHz to 2.54 MHz. Crystal oscillators for these frequencies are large and susceptible to shocks and damage because of their large, delicate internal structure. Instead of crystal, 1 MHz ceramic oscillator ISM95-3351AH was therefore selected for operation. Its phase noise is comparable to crystal oscillator, therefore no degradation in ADC operation is expected. Comparison of solutions is shown in the figure 6.7.

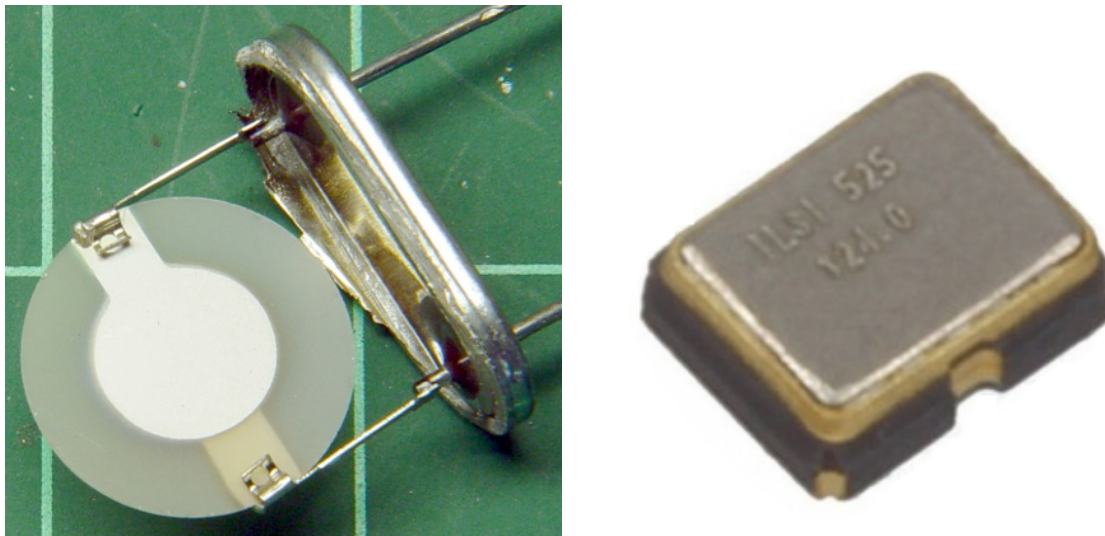


Figure 6.7: Left: Low frequency crystal oscillator. Source: [29]

Right: ISM95 ceramic oscillator. Source: [20]

6.4.6. Multiplexer

The multiplexer has two purposes: to multiplex current and voltage lines (3-wire readout).

As an analog multiplexer, ADG709 was chosen. Its radiation tests can be found in [19]. It is a double 1:4 mux, allowing for simultaneous current and voltage multiplexing. Its internal block diagram is shown in the figure 6.8

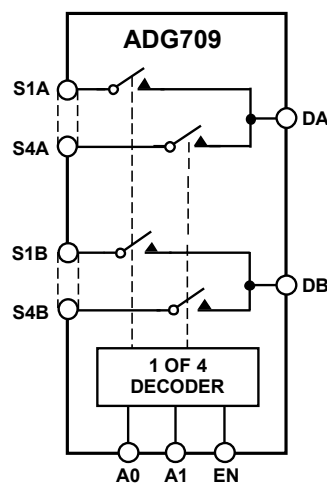


Figure 6.8: ADG709 internal block diagram. Source: [3]

Due to ESD diodes in CD4007, an additional current switch had to be added to cut off potential from n-MOS body diode. For this purpose, a simple 1-channel analog switch ADG849YKSZ was implemented.

6.4.7. Differential & common mode filter

The internal sampling frequency of ADC (for GAIN = 1 and $f_{clk} = 1$ MHz) is about 15.6 kHz. To eliminate aliasing and reduce readout noise, a low-pass differential filter should be implemented on ADC input.

A simple one-pole RC filter was selected. Its schematic can be found in the figure 6.9.

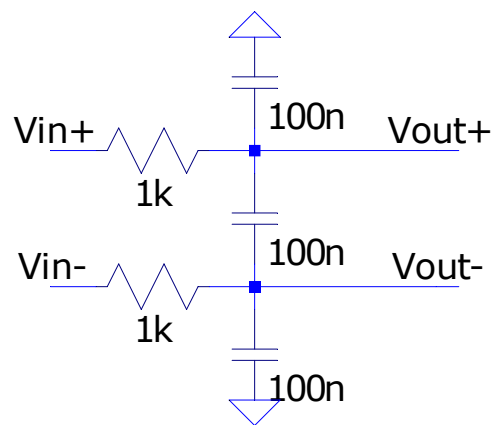


Figure 6.9: Low pass filter schematic.

Using AC analysis its frequency characteristic was obtained - figure 6.10. At half the sampling frequency, attenuation is about 22 dB.

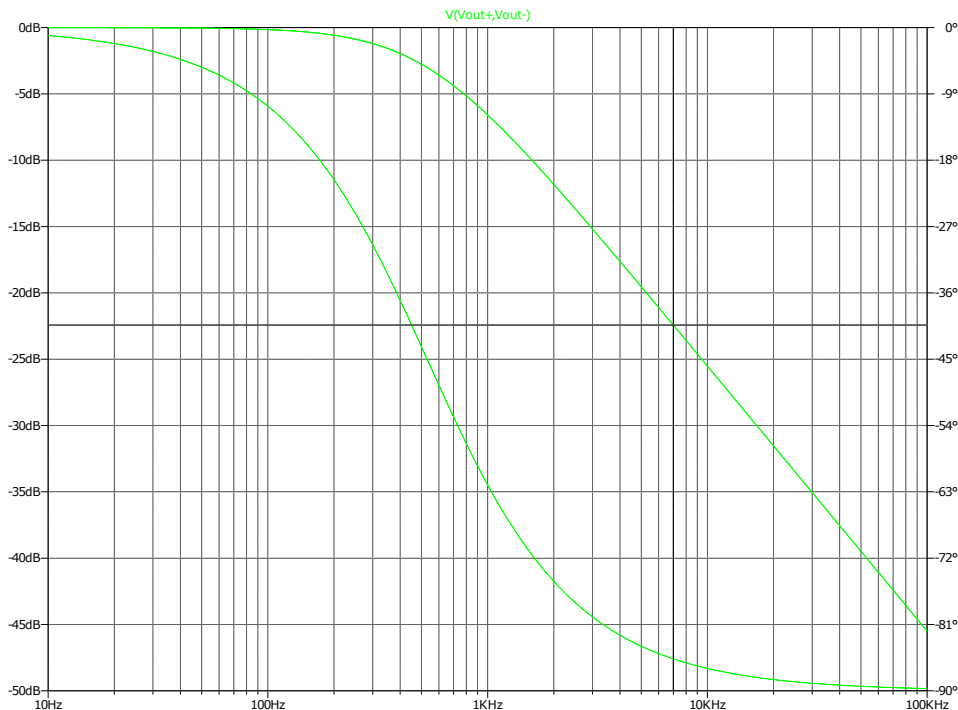


Figure 6.10: Low pass filter frequency characteristics.

6.4.8. Shielding

Because of noise requirements and near proximity of 0.5 W radio transmitter, EMI shielding was tested.

Proper pads for EMI shielding were placed on PCB. Its size depends on PCB layout, after routing it was decided to use the BMI-S-203 shield (figure 6.11). This shield should provide attenuation of about 50 dB at the transmitter frequency.

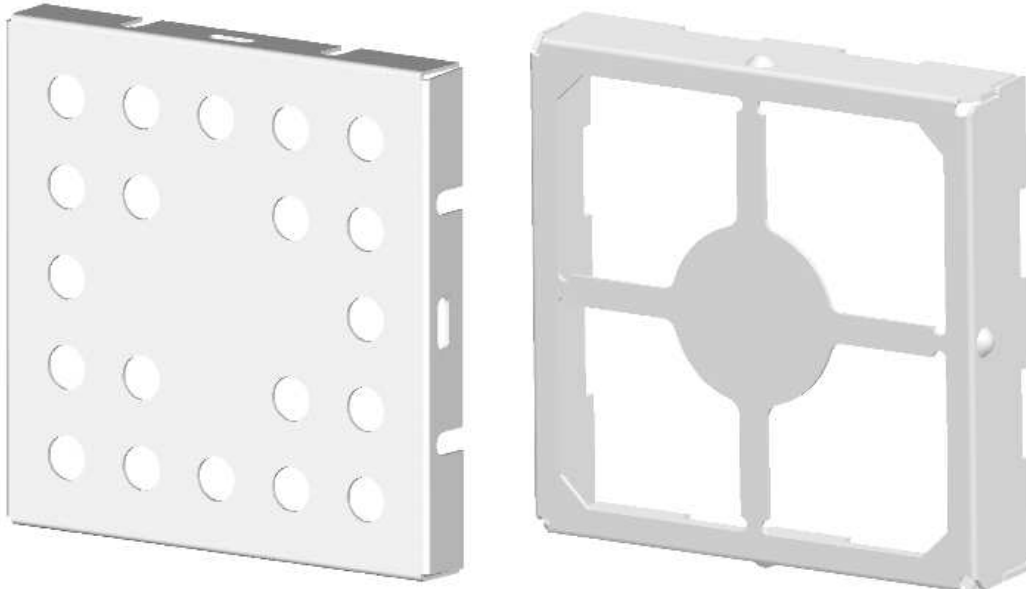


Figure 6.11: BMI-S-203 shield. Source: [24]

6.5. Digital

RadFET is mainly an analog sensor. However, LDO, MUX and ADC have to be controlled from the on-board microcontroller. On the other hand, the RadFET has to be accessible from OBC, to retrieve data and send them to the ground station.

6.5.1. Microcontroller

The main digital part of the design is the microcontroller. It will be responsible for:

- controlling analog part of the sensor,
- implementing FDIR in case of any failure,
- communicating with OBC to retrieve data.

Several options were considered, and the final choice was ATmega164PV-10AQ. More detailed comparison can be found in [32].

AVR devices are known for their simplicity, reliability and sparsity of bugs. Radiation tests were performed for ATmega series, showing their performance for up to 30 krad [6].

Features of this particular device:

- 1.8 V - 5.5 V supply voltage,
- 4 MHz clock,
- TQFP-44 package,
- 16 kB program memory,
- 1 kB SRAM

6.5.2. On-Board Computer interface

The interface to OBC is I^2C bus. Because the sensor can be turned off by cutting its voltage, proper buffering had to be implemented. For this purpose I^2C repeater PCA9517 was placed between OBC and the in-sensor microcontroller. Its functional diagram can be seen in the figure 6.12. From its datasheet: "The SDA and SCL pins are over voltage tolerant and are high-impedance when the PCA9517 is unpowered." [30]. Thanks to this, OBC can completely disable the sensor by simply cutting off power.

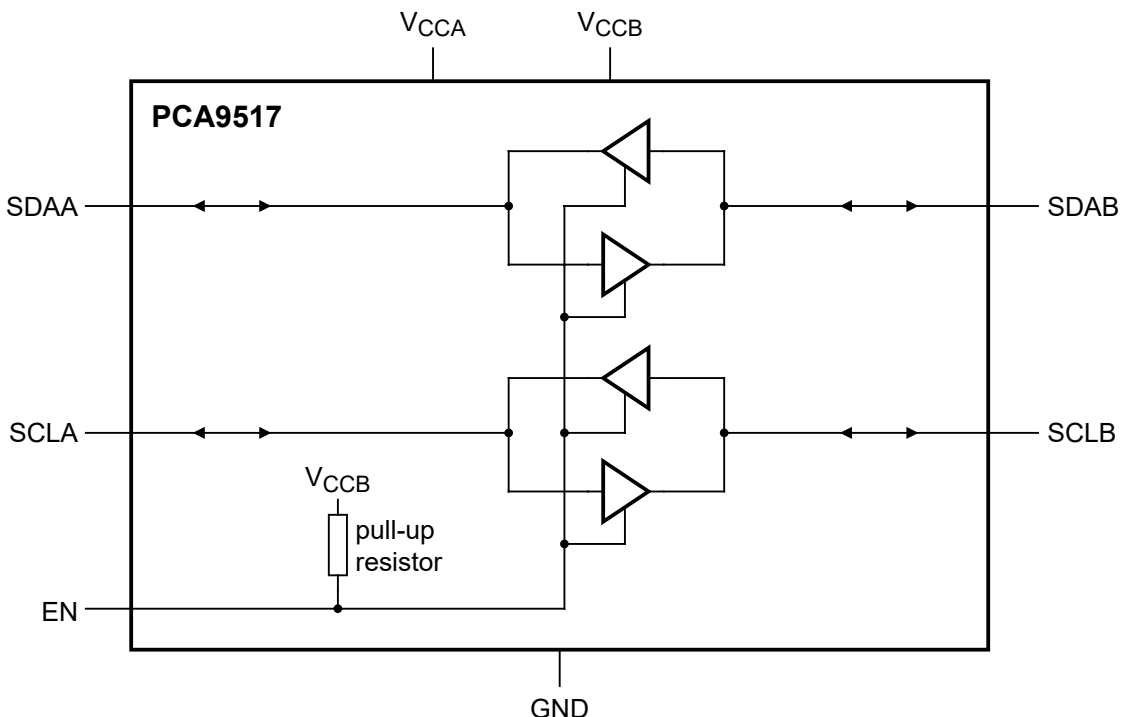


Figure 6.12: PCA9517 internal block diagram. Source: [30]

6.5.3. Watchdog

Because of possibility of Single Event Effects (described in section 3.2.1), mitigation of SEFI and SEU was implemented. It consists of a window watchdog, which reboots sensor in case of software being stuck in non-recoverable state. In case of failure, it will re-initialize sensor, which can recover in case any SEU in volatile (RAM) memory. In addition, in case of SEL it will pull down reset line, allowing for microcontroller internal circuitry to reset after power restore.

For this purpose, TPS3813-Q1 Processor Supervisor with window-watchdog was added to design. It is qualified to automotive operation, as well as it is recommended in Texas Instruments Defense Guide [40]. Internal block diagram is shown in the figure 6.13.

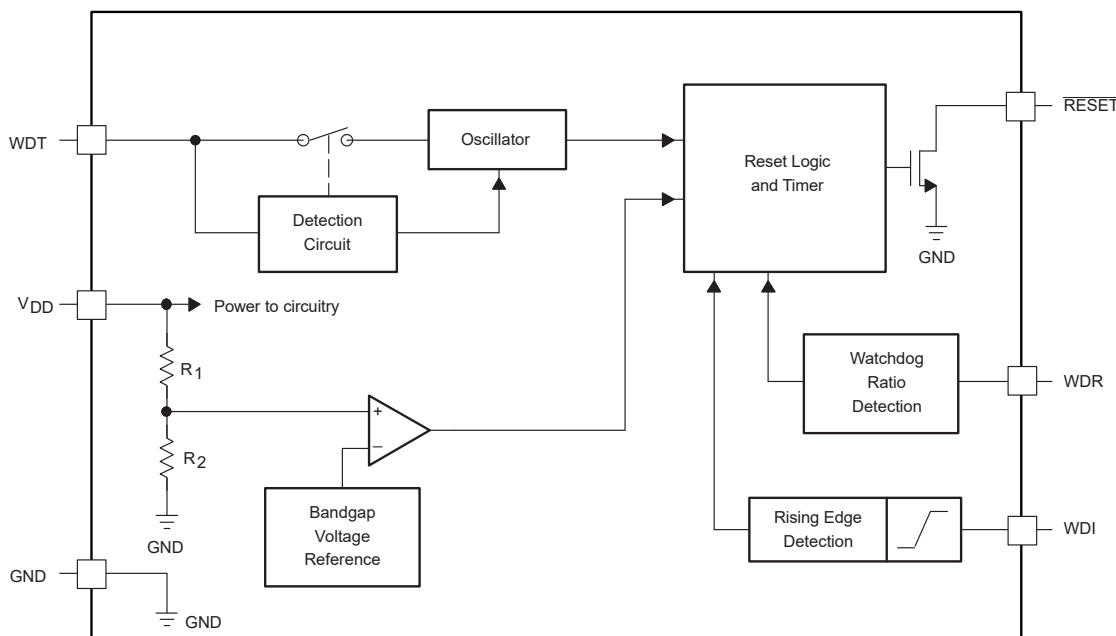


Figure 6.13: TPS3813 internal block diagram. Source: [41]

6.6. Final schematic

The top level schematic file can be seen in the figure 6.14. Ports represent physical connectors - to satellite bus and debug socket.

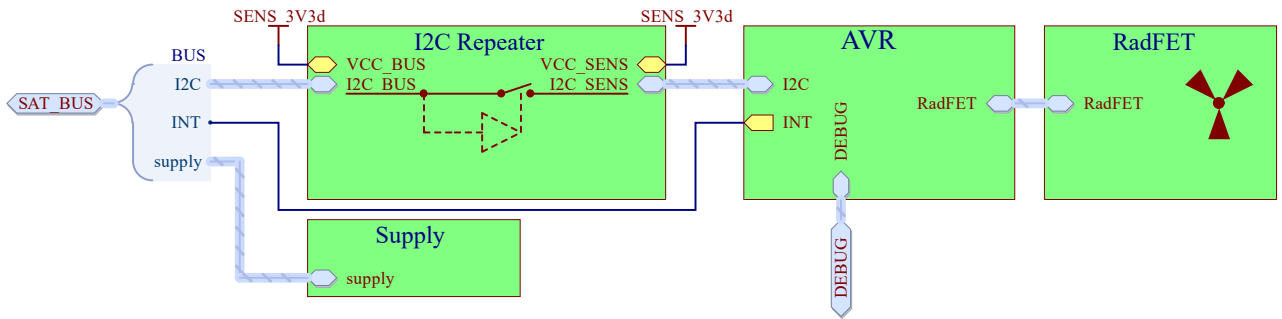


Figure 6.14: Top level schematic

"RadFET" makes up the analog part of the design. Its block diagram can be seen in the figure 6.15.

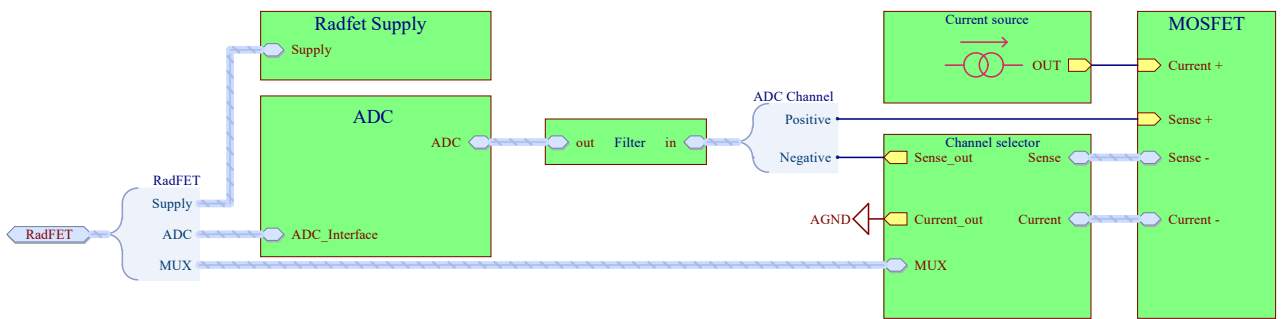


Figure 6.15: Sensor final schematic - analog part

6.7. PCB

The engineering model of the sensor was manufactured on a similar board to the flight model. It should represent the space required for this sensor, noise coupling and performance.

For schematic capture, PCB layout and DRC Altium Designer EDA software was used.

6.7.1. PCB materials

During the initial phase of the PW-Sat2 project it was decided that all self-made boards would be manufactured from FR4 laminate. Because most space-qualified PCBs are made of polyimide, it is very

hard (and expensive) to manufacture them. Apart from a higher glass transition temperature they do not provide many advantages.

Care should be taken to check for:

- vibration tolerance,
- gluing quality of multiple layer boards,
- outgassing coefficient.

With this in mind, a manufacturer of PCB was selected - Technoservice S.A.

6.7.2. PCB stack

Because outgassing of devices can be dangerous for turbomolecular pumps, it must be limited as much as possible. Therefore soldermask and overlay layers are not present in the design, and packages of used components have known outgassing coefficients.

Although this prototype board has 4 layers, the flight model board will be 6-layered. The PCB stack generated from Altium Designer is shown in the figure 6.16.

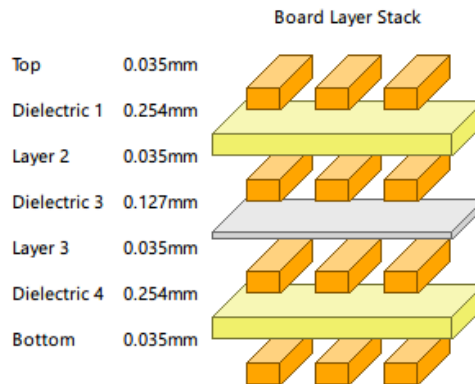


Figure 6.16: Sensor PCB stack

6.7.3. PCB layout

The PCB layout in the mixed signal board is very important. Ground potential shifts, induced noise, coupling between ground planes - all these effects were considered during the layout process.

Top & bottom layers

Components should be placed only on top and bottom layers, every net should be connected on internal layers. Because the model is built on a 4-layer board this design recommendation is not fulfilled - this will be forced on Flight Model. Final layout is shown in the figure 6.17.

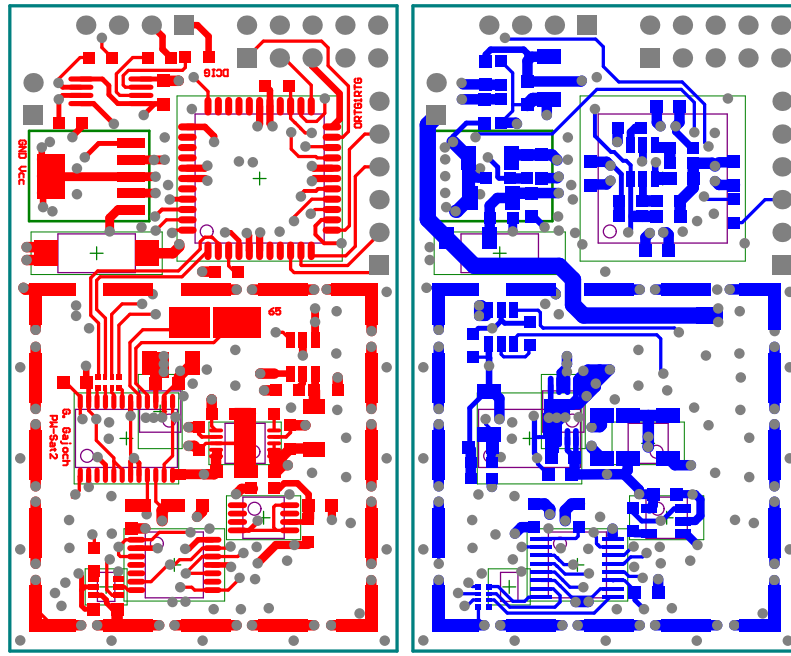


Figure 6.17: Top and bottom layer layout

Internal layers

One layer of the board was designed to serve completely as a ground plane. More specifically, two ground planes - an analog and a digital one, connected under ADC. The second internal layer provides routing space, but also has ground planes on it (due to PCB temperature bending, the PCB cannot have only one ground plane). Layout is shown in the figure 6.18.

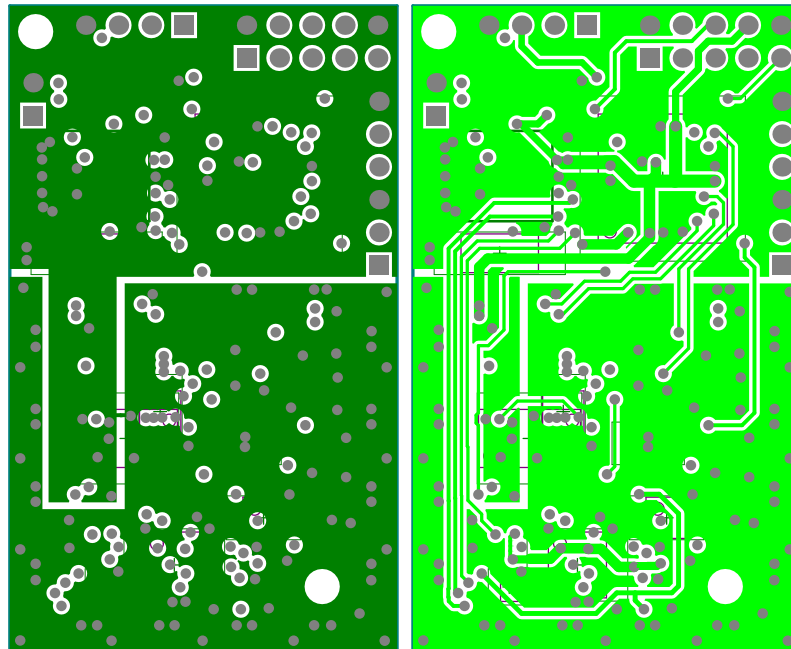


Figure 6.18: Internal layers layout

6.7.4. 3D model

Using the Altium designer and proper self-made libraries, a 3D model of board can be easily generated. In the figure 6.19 a 3D model with and without EMI shielding is shown.

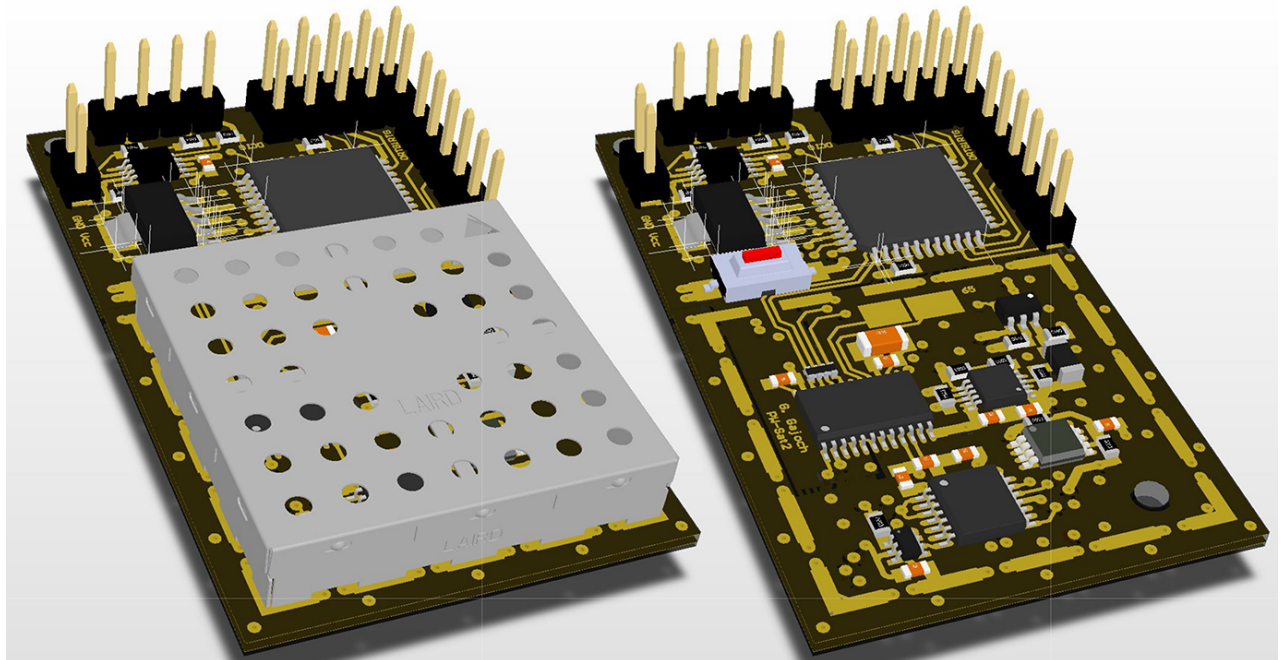


Figure 6.19: 3D view of engineering model with and without EMI shield

6.8. Software design

An important aspect of the sensor is its embedded software. It has to control data acquisition (LDO, ADC, MUX), check for validity and expose I^2C interface to OBC.

Because the main microcontroller is 8-bit AVR-core processor, software has to be highly optimized, especially for speed and data memory consumption. Available resources:

- 16 kB of FLASH,
- 1 kB of SRAM,
- 1 MHz clock frequency.

Software for the sensor was written in C++14, using the AVR-HAL library developed by the PW-Sat2 team. A schematic of software building blocks is shown in the figure 6.20.

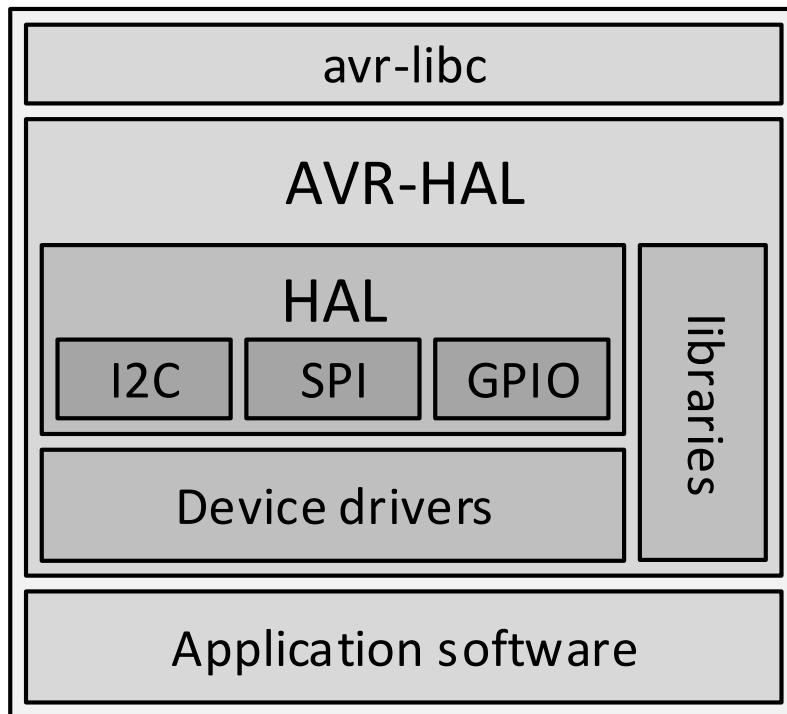


Figure 6.20: Sensor software diagram

6.8.1. AVR-HAL

AVR-HAL is a library created to ease software development on AVR microcontrollers. It was created by the PW-Sat2 team, with low overhead (in most modules zero-data usage), extensibility and modern software development languages and techniques (C++14, unit and integration testing) in mind. It was created for a specific purpose: embedded software development on-board PW-Sat modules (EPS, PLD, SunS). Therefore, only a few devices are officially supported (ATmega164, 165, 328), with extensible tests on existing platforms.

AVR-HAL consists of basic modules:

- C++14 libraries not existing in `avr-libc` (type traits, array, array_view),
- Hardware Abstraction Layer - identical low-level API for every ported device,
- Device Drivers - drivers for many used integrated circuits used on PW-Sat2,
- Debugging libraries - software created to allow unified debugging of many devices (serial port, command line interface, gdb connection etc).

Using AVR-HAL, writing application software is only high-level work, leaving all hardware access to the tested and proven library.

6.8.2. I^2C -slave interface

Cubesat standards define two I^2C lines along the satellite board stack, which most of the commercially available devices use. It was the easiest option for connecting the PLD board to OBC, so this communication bus was selected.

The sensor acts as a slave on the I^2C bus. Communication protocol is based on a request-reply manner, with the interrupt pin state acting as a notification.

When OBC wants to gather data from the sensor it will do following tasks in order:

- send measurement start request to sensor (table 6.1),
- wait until conversion is completed (pulse on interrupt line is triggered),
- read data from sensor internal memory (table 6.2).

Table 6.1: Start measurement command

START	0x20+W	0x80	STOP
-------	--------	------	------

Table 6.2: Data readout command

START	0x20+W	0x00	REP-START	0x20+R	(...data...)	STOP
-------	--------	------	-----------	--------	--------------	------

6.8.3. Measurement algorithm

RadFET sensor

The sensor, after receiving "start measurement" command (table 6.1) does following steps:

- enable LDO,
- wait for power line stabilization,
- for each channel in [MOS0, MOS1, MOS2, TEMPERATURE]:
 - select proper MUX switch,
 - enable MUX,
 - wait for stabilization,
 - read ADC value,

- disable MUX
- disable LDO,
- make a positive pulse on interrupt line, informing OBC about conversion finish.

OBC

When OBC wants to read data from the sensor (issued by telecommand from ground station) it performs the following steps:

- enable PLD power by sending proper command to EPS,
- send "start measurement" command to RadFET,
- wait for trigger on interrupt line (external interrupt pin),
- send "data readout" command and store data in memory,
- disable power for PLD board

6.9. Assembly

For the final model, proper ECSS standards will be applied during soldering and integration. On the engineering model proper tools and techniques should be tested to eliminate unnecessary problems later on.

Equipment used during soldering and integration is compliant with ECSS standards, the same tools are used on flight hardware:

- Weller WMRP station,
- 63 % Sn/37 % Pb 0.2 mm soldering wire,
- Alpha RMA - ROL0 flux,
- ESD-protected workstation and tools.

6.10. Finished sensor

Photo of sensor after integration can be seen in the figures 6.21 and 6.22.

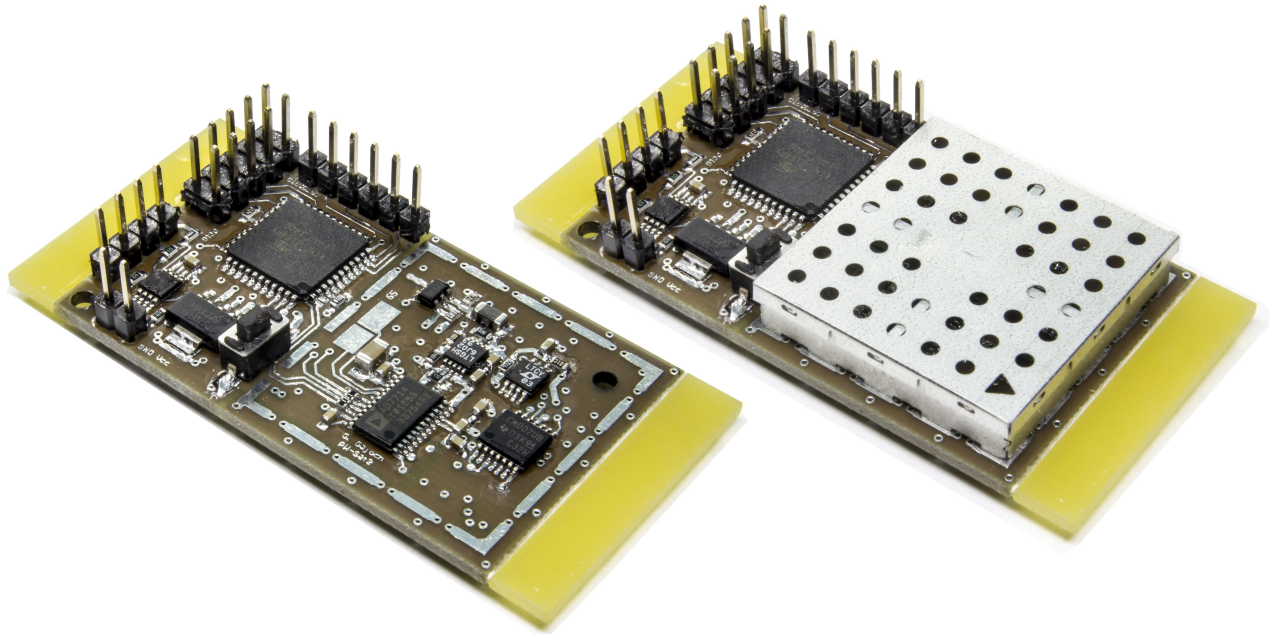


Figure 6.21: Integrated sensor without and with EMI shield

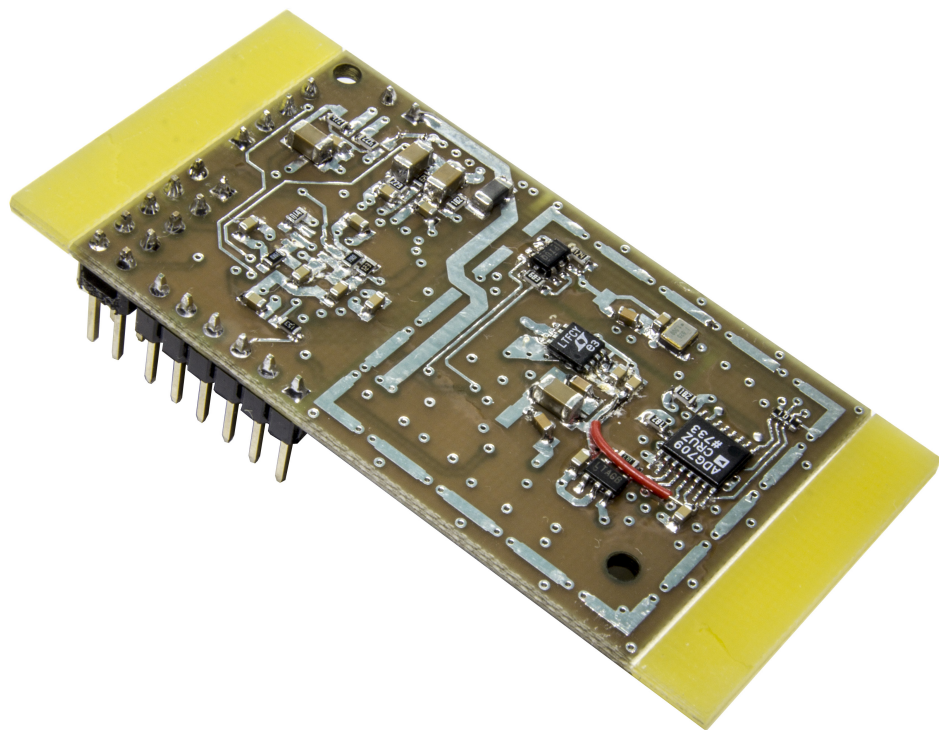


Figure 6.22: Integrated sensor - bottom

7. Sensor tests

7.1. Power

7.1.1. LDO stabilisation

Voltage after LDO was measured against time, to calculate the delay between power enablement and measurement start. The time-domain graph is shown in the figure 7.1. Delay was estimated to be around 1 s.

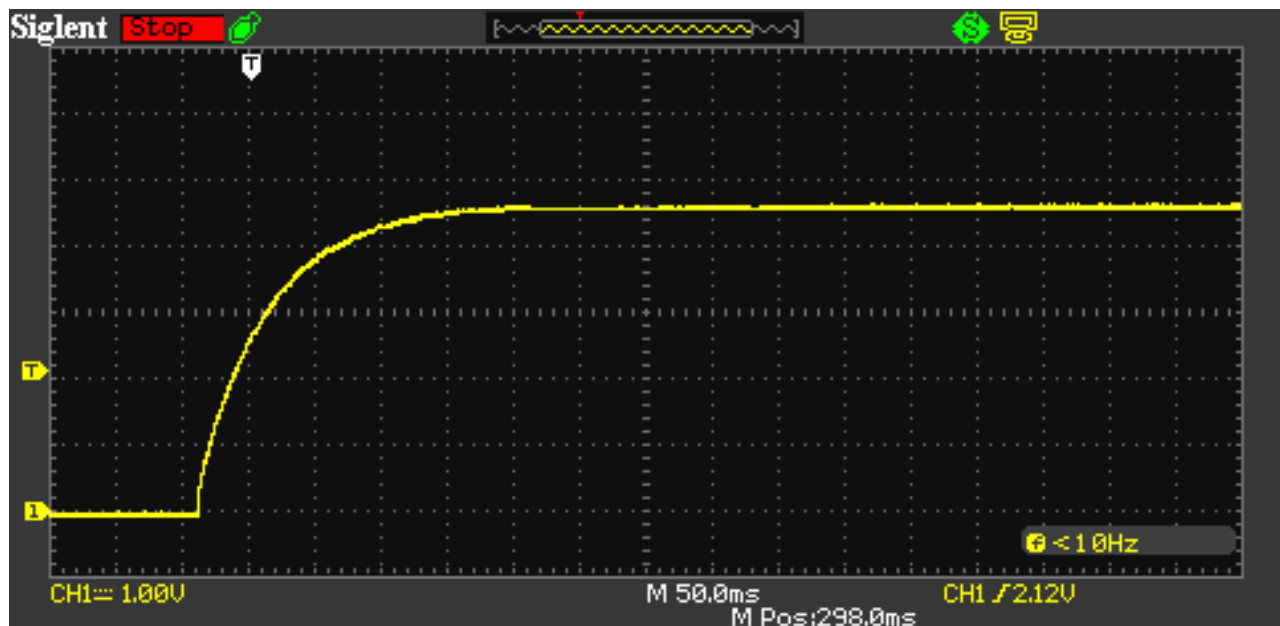


Figure 7.1: LDO rise time

7.1.2. Power consumption

The current drawn during readout is about 25 mA at 5 V rail, so the power consumption of the sensor equals to 0.125 W.

7.2. Current source

Current source was tested on HP 34970A - 6 1/2 digit multimeter, with 200 power line cycle integration enabled.

7.2.1. Noise

The noise of the current source was measured for a long period of time, taking a sufficient number of samples. Results (figure 7.2) show that the noise floor is below specification for this meter.

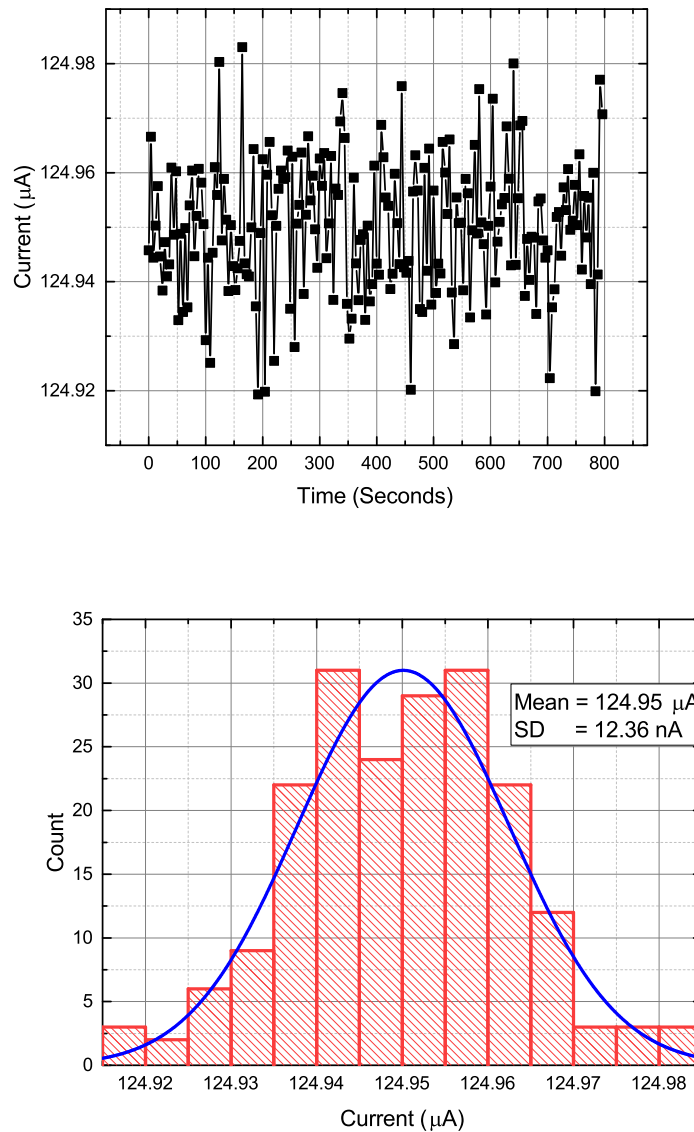


Figure 7.2: Current noise measurement

7.2.2. Load range

Output characteristics was measured in identical manner as in simulation. Simulation and build models show the same range of stability - confirming both the design and simulation. The current source works as intended for loads between $1.4\text{ k}\Omega$ and $22.5\text{ k}\Omega$ (figure 7.3).

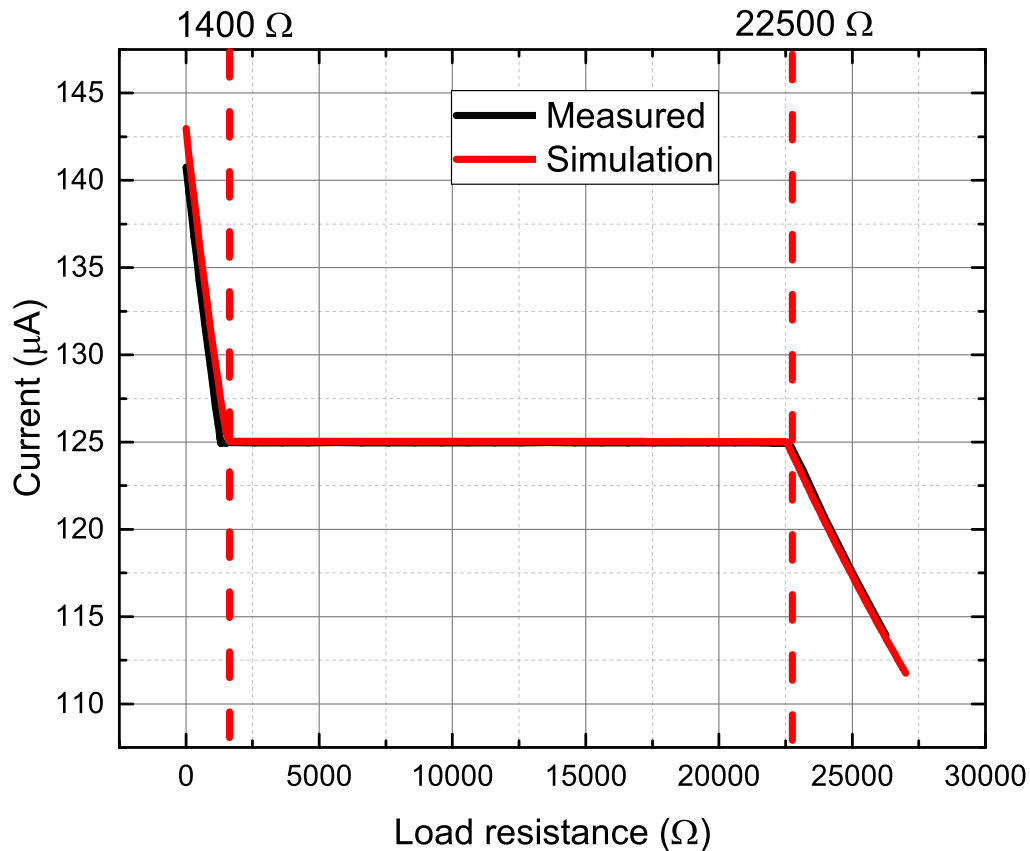


Figure 7.3: Current source output characteristics

7.2.3. Temperature stability

Temperature was swept from 20 to 70°C , no detectable changes were measured by the available meter, therefore it is assumed that current source fluctuates less than about 20 nA in this temperature range.

7.3. MOS settling

After enabling the measurement channel for the threshold voltage it takes a lot of time to fully stabilize its value. Instead of pre-enabling, same time method was used. ADC takes measurement of threshold voltage at precisely specified time after enabling power. In the figure 7.4 10 runs of measured voltage vs time are plotted, proving this method is stable within 20 μ V.

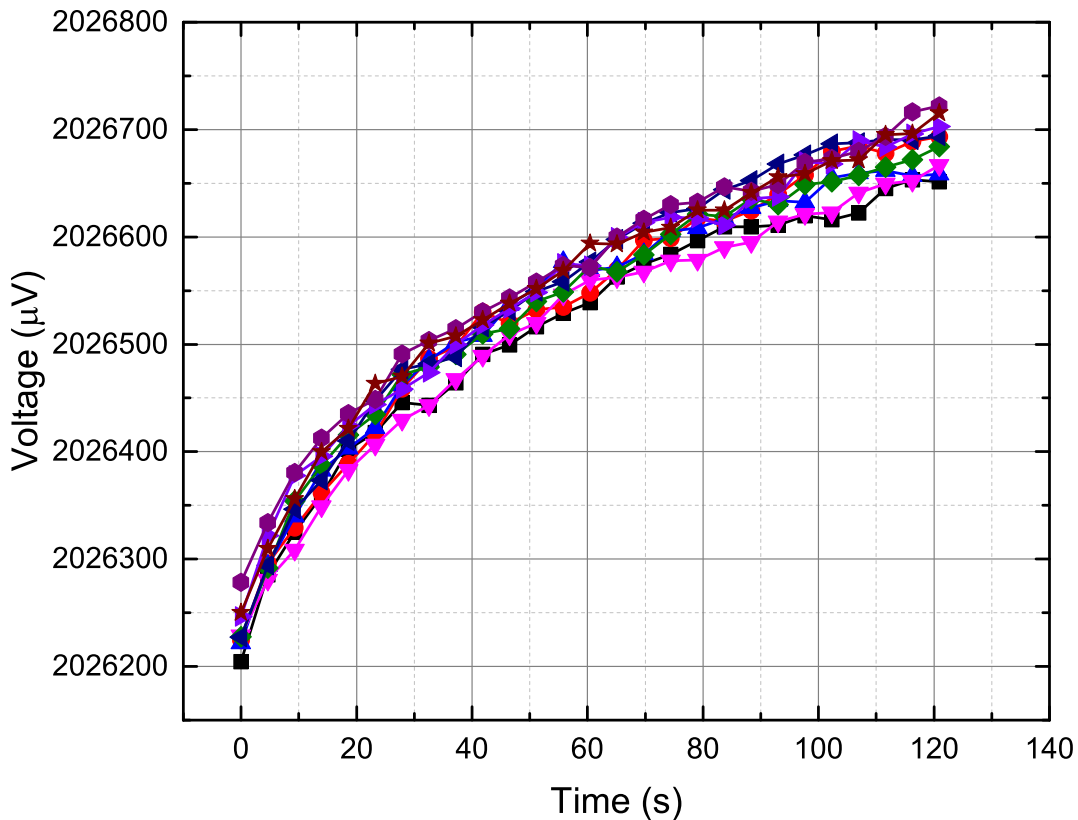


Figure 7.4: 10 runs of MOS voltage setting

7.4. Measurement noise

The most important noise figure is system noise - ADC reading noise floor during nominal operation. Because even the smallest temperature changes cause the ADC reading to shift (due to threshold/-diode voltage shift), this effect had to be eliminated to measure noise. For this purpose a DC notch filter was used in post-processing, to eliminate any DC bias during measurement. The sampling frequency of the ADC was its nominal rate of 0.25 Hz. An example of filtration is shown in the figure 7.5.

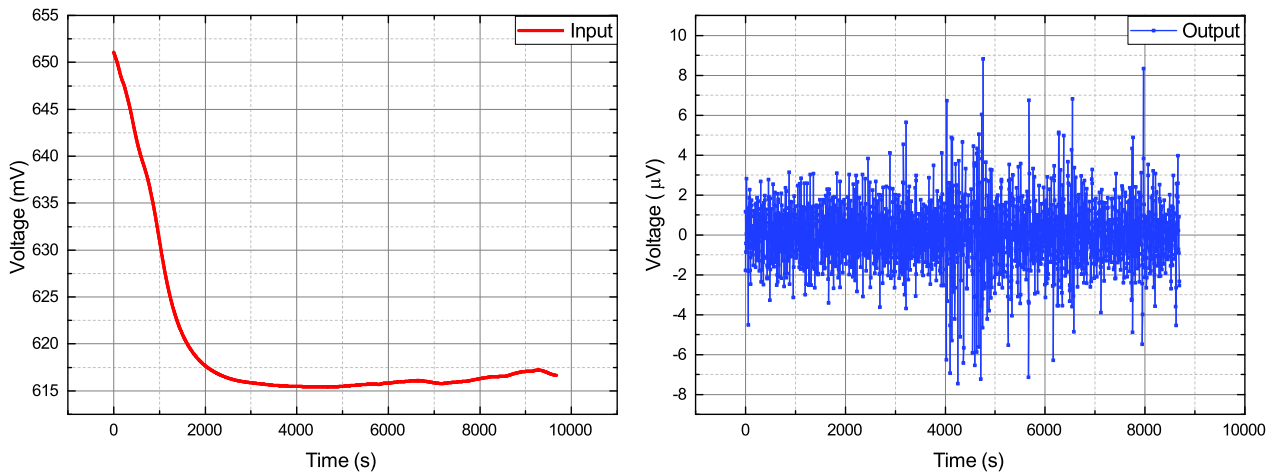


Figure 7.5: Input and output of DC notch filter

7.4.1. Diode

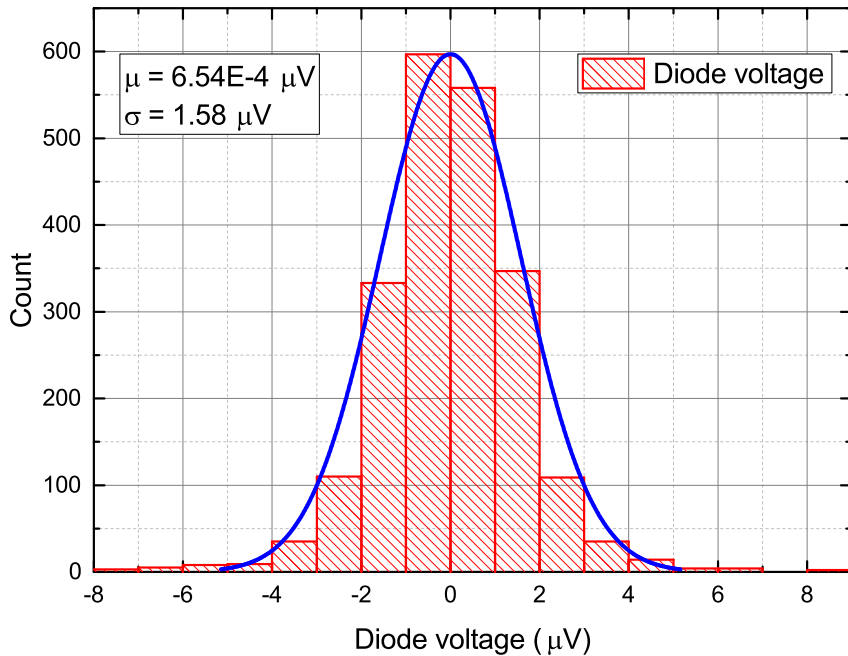


Figure 7.6: Measured noise on body temperature channel

Noise on the temperature measurement channel has a standard deviation of $1.58 \mu\text{V}$

7.4.2. Threshold voltage

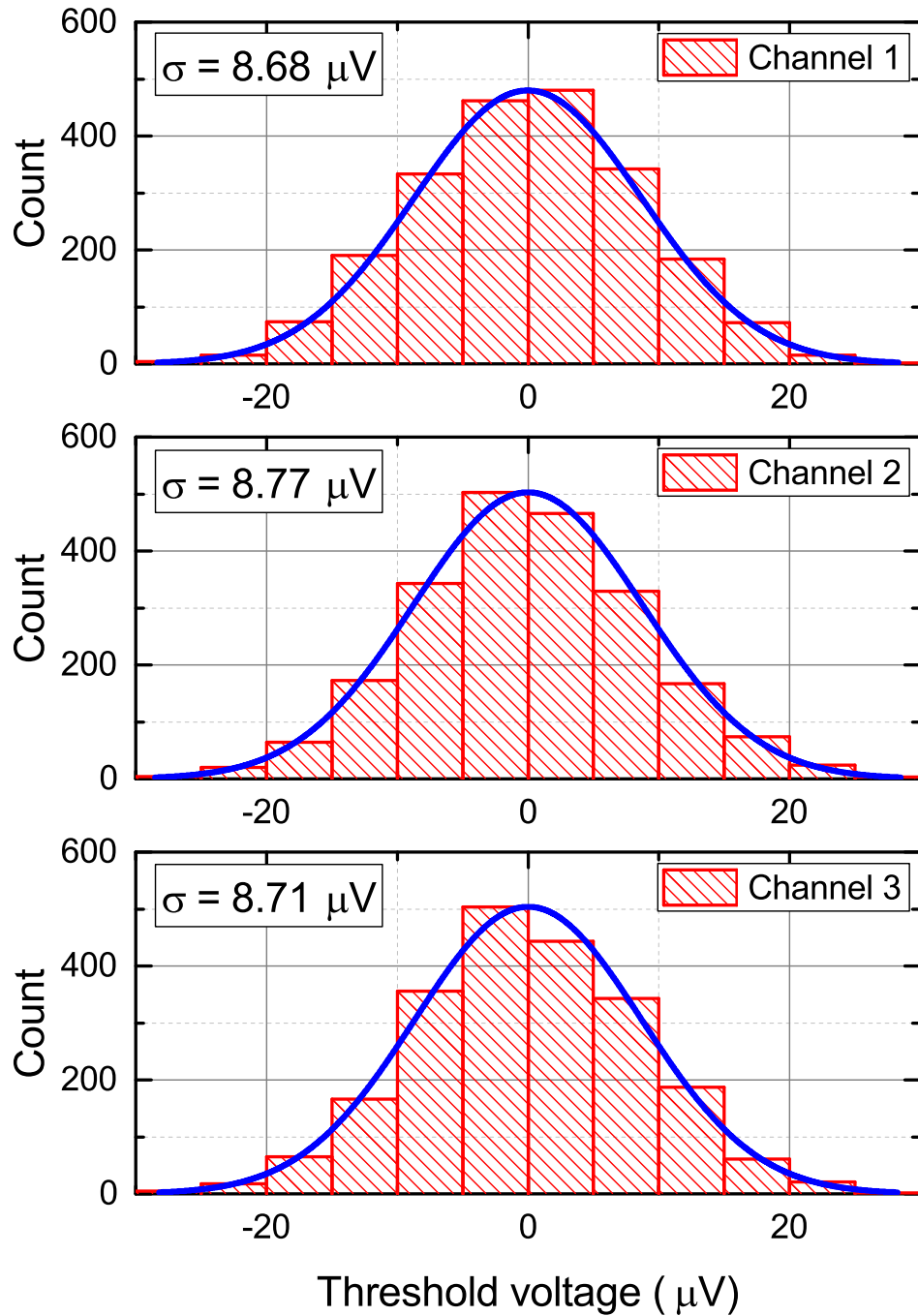


Figure 7.7: Measured noise on body temperature channel

Noise on the threshold voltage measurement channel has standard deviations of $8.68 \mu\text{V}$, $8.77 \mu\text{V}$, $8.71 \mu\text{V}$.

7.4.3. Interpretation

Because the only difference between the temperature and threshold voltage channels is the semiconductor itself, the noise source can be estimated from the significant difference between them.

The dependence between threshold voltage and drain current for this type of transistor was measured by M. Gumiela:

$$I_D [\mu A] = 410.376 \cdot (V_{TH} - 1.56457)^2 \quad \text{Source: 5.5}$$

$$\frac{d}{dV_{TH}} I_D = 820.75 \cdot (-1.56 + V_{TH}) = 439.46 \mu A/V \quad @ \text{operating point}$$

$$dI_d = 3.82 \text{ nA}$$

Estimated equivalent current source have RMS value of $I_{N \text{ RMS}} = 3.82 \text{ nA}$.

This value is the same order of magnitude as calculated: reference voltage LT1634 has low-frequency noise of $U_N = 15 \mu V$ [25], this value is sensed directly across a series resistor, therefore $I_{NOISE} = U_N/R = 1.5 \text{ nA}$. Additional noise equation can originate from different parts of the circuit, thermal and shot noise etc.

7.5. Temperature characteristics

By placing the sensor in a thermal chamber and sweeping the temperature from 0 °C up to 75 °C temperature dependency charts were obtained for the device.

7.5.1. Diode channel

The diode response (figure 7.8) is almost ideally linear.

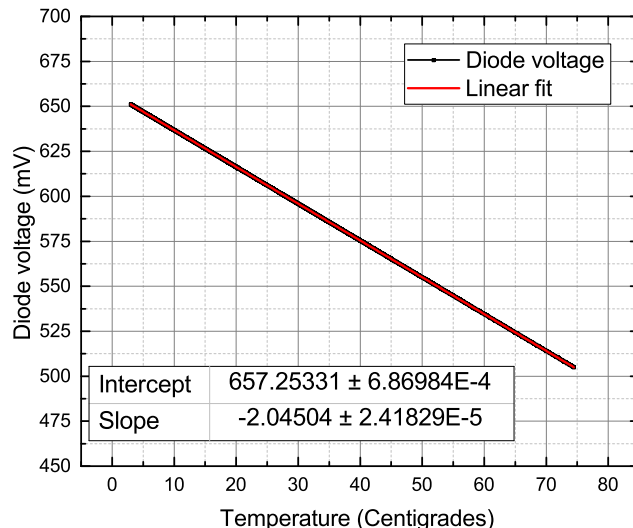


Figure 7.8: Body diode temperature dependency

7.5.2. Threshold voltage channels

The threshold voltage (figure 7.9) tends to be non-linear, but it can be approximated by a quadratic function. Equation used: $V_{TH} = a \cdot t^2 + b \cdot t + c$, fitted parameters are shown in the table 7.1.

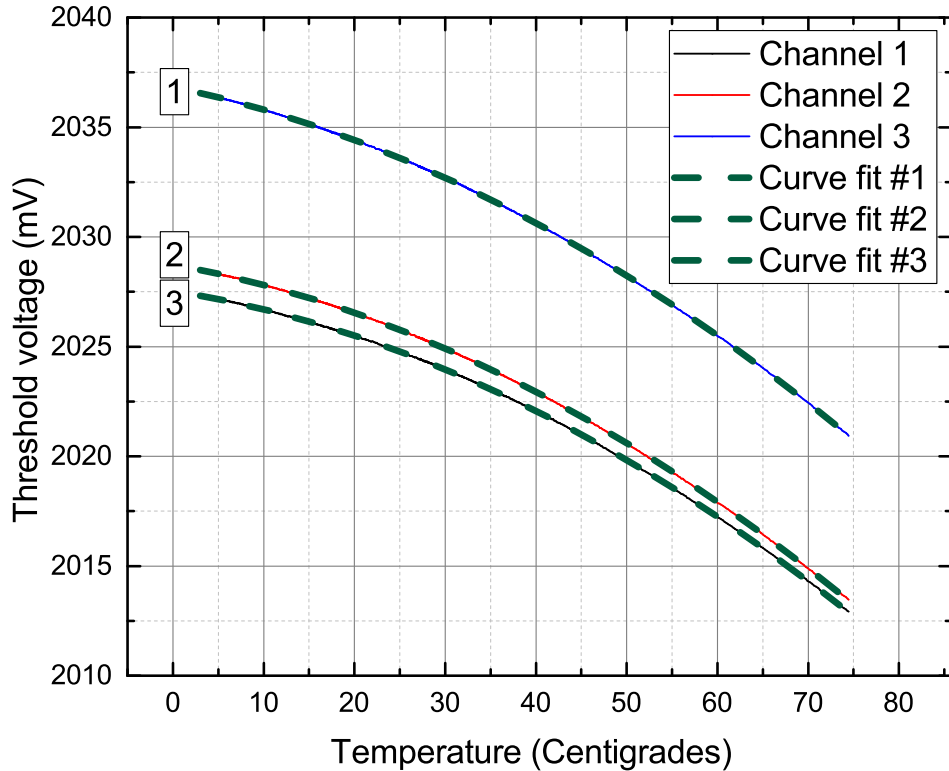


Figure 7.9: Threshold voltage temperature dependency

Table 7.1: Threshold voltage temperature dependency

Channel	a	b	c
ch 1	$-0.00174 \pm 1.17011e - 6$	$-0.06692 \pm 8.33551e - 5$	2027.53424 ± 0.00125
ch 2	$-0.00176 \pm 1.07318e - 6$	$-0.07437 \pm 7.64496e - 5$	2028.72804 ± 0.00114
ch 3	$-0.00169 \pm 1.12071e - 6$	$-0.08736 \pm 7.98355e - 5$	2036.83689 ± 0.00119

7.6. Temperature compensation stability

The sensor should be compensated for temperature, with the assumption that temperature characteristic curves will not change during irradiation.

During temperature sweep, data was gathered and post-processed, applying thermal compensation (given by charts 7.8 and 7.9). In full sensing range, the sensor output shifts off the maximum 104 μ V, which reflects TID measurement accuracy of about ± 1 rad. Note that TID dependency was not tested, but assumed according to [28]. Detailed accuracies are listed in the table 7.2.

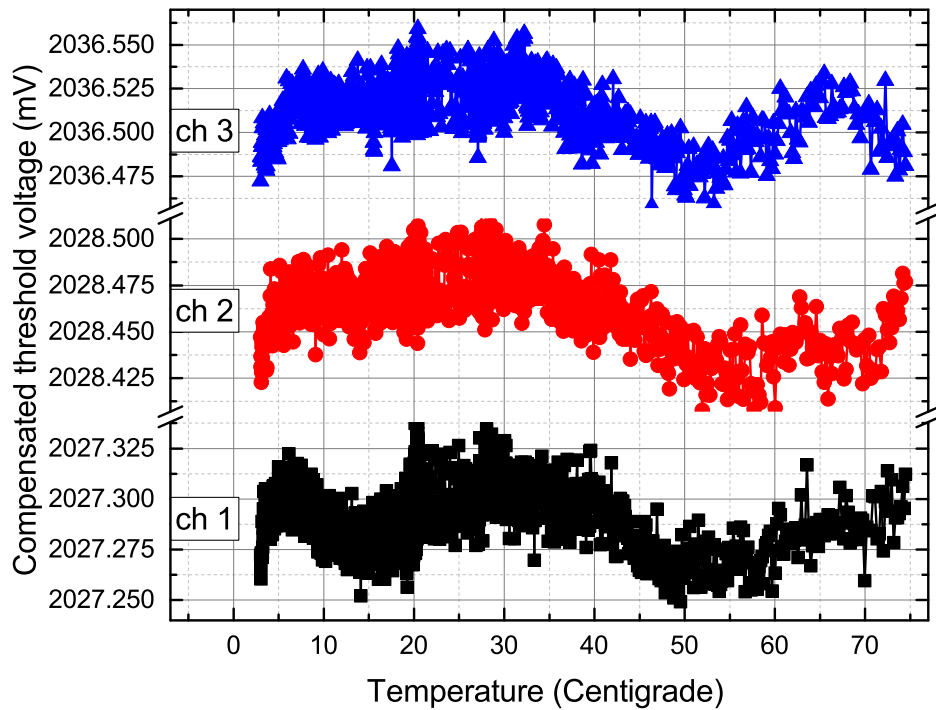


Figure 7.10: Threshold voltage temperature compensation

Table 7.2: Temperature compensation results

Channel	Standard deviation	Maximum difference	Accuracy (3σ)
ch 1	15.13 μ V	89.40 μ V	± 0.0108 Gy = ± 1.08 rad
ch 2	16.27 μ V	103.24 μ V	± 0.0109 Gy = ± 1.09 rad
ch 3	15.36 μ V	101.26 μ V	± 0.0103 Gy = ± 1.03 rad

8. Future work

This chapter briefly describes the required steps for the sensor to be able to fly on-board PW-Sat2.

8.1. Qualification model

Firstly, the sensor will be implemented on a PC-104 factor board, together with all final components and procedures. The model shown is taken from the design process (figure 8.1).

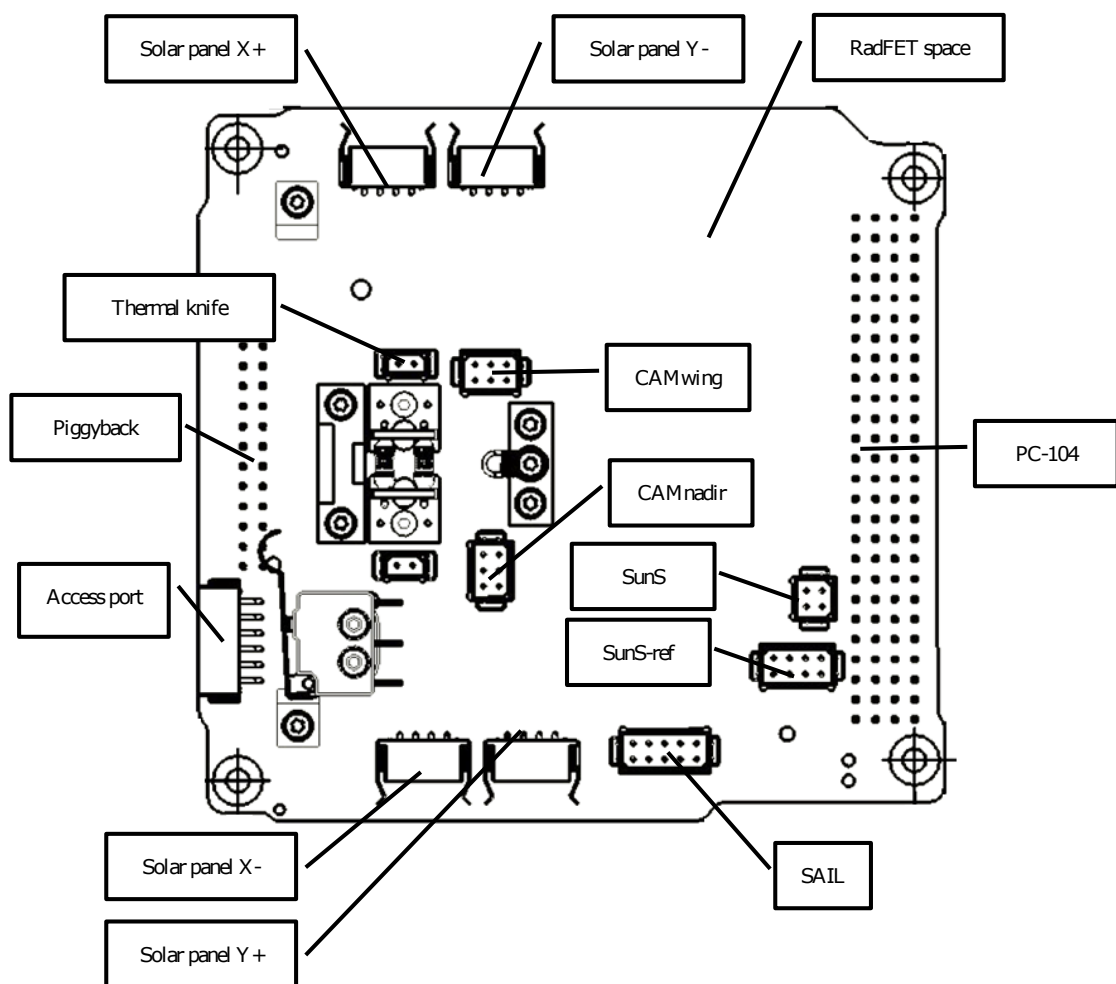


Figure 8.1: PLD board with connector and space designed for RadFET

On this model all software tests (on flat-sat) will be carried out, as well as the final confirmation of design (thermal, radiation and time-stability tests). This board will qualify sensor design and software for flight use.

8.2. Flight model

In the end, a final flight version of the PCB will be manufactured. In principle, it should be identical to the Qualification Model, but the handling procedures will be much more strict. Additionally, on the flight model, only thermal calibration will be made, without further stress-testing. During integration, the final version of the sensor on PC104-board will be placed on the electronics stack inside PW-Sat2.

9. Summary

The engineering model of the sensor was designed and preliminarily tested. This is a solid foundation to further work, which will result in the flight-ready version of the sensor. This model allowed for testing of the concept and possible solutions of sensor components, proving the design.

Tests have proven the fidelity of measurements - assumed resolution and range are beyond the requirements. Designed sensor parameters are shown in table 9.1.

Table 9.1: Finished sensor parameters

Parameter	Result
Sensor resolution	0.003 rad,
Sensor accuracy	1 rad,
Sensor range	10 krad,
Operating temperature range	0 °C to 70 °C,
Communication protocol	I^2C ,
Sensor supply voltage	5 V,
Sensor power consumption	0.125 W,
Radiation tolerance	> 15 krad

This thesis resulted in a fully integrated, ready to use sensor which can be used as a preliminary calibration check model. It was designed for a space environment, with the limitations and requirements of CubeSat satellite in mind. During testing, the sensor design was proved through the conduction of tests. Moreover, since its size and requirements on the bus have been limited, broader possibilities of manufacturing this sensor as a separate module exist for other CubeSat missions.

As a next step, this model has to be tested more thoroughly - especially radiation tests and calibration. Later, qualification and flight models will be manufactured, hopefully leading to sensor launch on PW-Sat2 satellite at the end of year 2017, where it can be tested in target space conditions.

Bibliography

- [1] . *Radiation environment*. [Online; accessed 20-Nov-2016]. European Space Agency,
- [2] Analog Devices. *AD7714 datasheet*. <http://www.analog.com/media/en/technical-documentation/data-sheets/AD7714.pdf>. [Online; accessed 20-Nov-2016].
- [3] Analog Devices. *ADG709 datasheet*. http://www.analog.com/media/en/technical-documentation/data-sheets/ADG708_709.pdf. [Online; accessed 20-Nov-2016].
- [4] Analog Devices. *Image of a functional diagram of CD4007 integrated circuit*. <https://wiki.analog.com/university/courses/electronics/electronics-lab-28>. [Online; accessed 20-Nov-2016].
- [5] Arsalan M., Shamim A., Tarr N.G., Roy L. “Miniaturized, low power FGMOSFET radiation sensor and wireless dosimeter system”. Pat. US8519345 B2.
- [6] Boterenbrood H. , Hallgren B. *SEE and TID Tests of the Embedded Local Monitor Board with the ATMEGA128 processor*. Internal Working Note. CERN ATLAS.
- [7] Burr-Brown, ed. *APPLICATION BULLETIN: Make a precision current source or sink*.
- [8] California Polytechnic State University, San Luis Obispo. *CubeSat Design Specification Rev. 13*. 2014.
- [9] Carvajal M.A., Simancas F., Guiradob D., Vilchesb M., Lallenac A.M., Palmaa A.J. “A compact and low cost dosimetry system based on MOSFET for in vivo radiotherapy”. *Sensors and Actuators: A Physical* 210 (2014), 146 — 152.
- [10] ESA. *European Cooperation for Space Standardization*. <http://ecss.nl/>. [Online; accessed 20-Nov-2016]. 2016.
- [11] ESA. *European Space Components Information Exchange System*. <https://escies.org/>. [Online; accessed 20-Nov-2016]. 2016.

- [12] ESA. *SPace ENvironment Information System*. <http://www.spenvis.oma.be/>. [Online; accessed 20-Nov-2016]. 1997.
- [13] ESA-ESTEC. *ECSS-E-ST-20-07C: Electromagnetic compatibility*.
- [14] ESA-ESTEC. *ECSS-Q-ST-60-15C: Radiation hardness assurance - EEE components*.
- [15] ESA-ESTEC. *ECSS-Q-ST-70-04C: Thermal testing for the evaluation of space materials, processes, mechanical parts and assemblies*.
- [16] ESCIES. *ESCC Radiation Test Methods and Guidelines - Total Dose Steady-State Irradiation Test Method*.
- [17] Fuller L. F. Dr. *Dr. Fuller homepage*. <https://people.rit.edu/lffeee/>. [Online; accessed 20-Nov-2016]. 2015.
- [18] Gumiela M. “Development of calibration stand for MOSFET transistors working as ionizing radiation sensors”. Engineering thesis. AGH University of Science and Technology.
- [19] Hiemstra D. M. *IEEE radiation tests 1992-2009*. IEEE.
- [20] ILSI America. *ISM95 Series datasheet*. http://ilsiamerica.com/wp-content/uploads/2015/10/ISM95_Series.pdf. [Online; accessed 20-Nov-2016].
- [21] Irom F. , Shri G. A. *Compendium of Single-Event Latchup and Total Ionizing Dose Test Results of Commercial Analog to Digital Converters*. Jet Propulsion Laboratory, California Institute of Technology.
- [22] Jaksic A., ed. *RADFET development and calibration*. CNES/ESA Final Presentation Days. Devices and Systems for Dosimetry, Tyndall National Institute.
- [23] Johnson N. L. *The disposal of spacecraft and launch vehicle stages in Low Earth Orbit*. NASA Johnson Space Center.
- [24] Laird Technologies. *Board Level Shields Catalog*. <http://cdn.lairdtech.com/home/brandworld/files/Board%20Level%20Shields%20Catalog%20Download.pdf>. [Online; accessed 20-Nov-2016].
- [25] Linear Technology. *LT1634 datasheet*. <http://cds.linear.com/docs/en/datasheet/1634ff.pdf>. [Online; accessed 20-Nov-2016].
- [26] Linear Technology. *LT3042 datasheet*. <http://cds.linear.com/docs/en/datasheet/3042fa.pdf>. [Online; accessed 20-Nov-2016].
- [27] Makowski D. *The Impact on Electronic Devices with the Special Consideration of Neutron and Gamma Radiation Monitoring*. A thesis of Ph.D., Department of Microelectronics and Computer Science, Technical University of Lodz. 2006.

- [28] Martínez-García M.S., Simancas F., Palma A.J., Lallena A.M., Banqueri J., Carvajal M.A. “General purpose MOSFETs for the dosimetry of electron beams used in intra-operative radiotherapy”. *Sensors and Actuators: A Physical* 210 (2014), 175 — 181.
- [29] Nisley E. *Opening a Quartz Crystal Can: Effects Thereof*. <https://softsolder.com/2010/05/15/opening-a-quartz-crystal-can-effects-thereof/>. [Online; accessed 20-Nov-2016]. 2015.
- [30] NXP. *PCA9517 datasheet*. http://www.nxp.com/documents/data_sheet/PCA9517.pdf. [Online; accessed 20-Nov-2016].
- [31] Panwar L., Chaudhary H.S., Vaijapurkar S.G., Bohra D., Bhatnagar P.K. “Silicon PIN diode neutron dosimetry”. *IJPAP Vol.48(11)* 48 (2010), 813 — 816.
- [32] PW-Sat2. *Electrical Power Supply Report - Critical Design Review*. 2016.
- [33] PW-Sat2. *Mission Analysis Report - Critical Design Review*. 2016.
- [34] PW-Sat2. *Thermal Control System - Critical Design Review*. 2016.
- [35] Riebeek H., NASA. *Catalog of Earth Satellite Orbits*. <http://earthobservatory.nasa.gov/Features/OrbitsCatalog/>. [Online; accessed 24-Nov-2016]. 2009.
- [36] S., R. G. “pMOS dosimeters (RADFETs)” (2015). Applied Physics Laboratory, Faculty of Electronic Engineering, University of Nis, Serbia.
- [37] SpaceX. *A photo of Falcon9*. <http://www.spacex.com/falcon9>.
- [38] SpaceX. *Falcon 9 Launch Vehicle - PAYLOAD USER'S GUIDE Rev 2*.
- [39] Taylor A. *The 'Model Philosophy' Used by Space Engineering Companies*. http://www.eetimes.com/document.asp?doc_id=1318780. [Online; accessed 24-Nov-2016]. 20013.
- [40] Texas Instruments. *Defense Guide*. <http://www.ti.com/lit/sg/sgzt007a/sgzt007a.pdf>. [Online; accessed 20-Nov-2016].
- [41] Texas Instruments. *TPS3813-Q1 datasheet*. <http://www.ti.com/lit/ds/symlink/tps3813-q1.pdf>. [Online; accessed 20-Nov-2016].
- [42] Uwarowa I.; Ciechowska K.; Gajc K.; Gawin M.; Kania M.; Kuligowski P.; Łukasik A.; Paćzkowska D.; Perczyński F.; Pilarski K.; Roszkowski D.; Ryszawa E.; Sobiecki M., ed. *Deorbit Sail for PW-Sat2 satellite mission – low energy consumption and high efficiency system*. Deorbit Device Competition.
- [43] Warsaw University of Technology. *PW-Sat2 website*. <http://pw-sat.pl/>. [Online; accessed 20-Nov-2016]. 2016.

- [44] Świetlik M. *A render of PW-Sat2 satellite*. Internal resources of the PW-Sat2 team.
- [45] Wolpert D., Ampadu P. *Managing Temperature Effects in Nanoscale Adaptive Systems*. 2012.